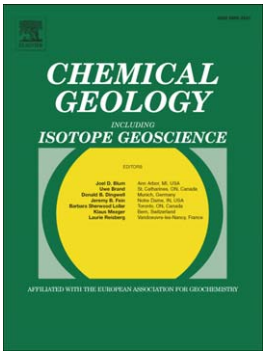

A combined Y/Ho, high field strength element (HFSE) and Nd isotope perspective on basalt weathering, Deccan Traps, India

M.G. Babechuk, M. Widdowson, M. Murphy, B.S. Kamber

PII: S0009-2541(14)00593-2
DOI: doi: 10.1016/j.chemgeo.2014.12.017
Reference: CHEMGE 17442

To appear in: *Chemical Geology*

Received date: 20 June 2014
Revised date: 15 December 2014
Accepted date: 17 December 2014

Please cite this article as: Babechuk, M.G., Widdowson, M., Murphy, M., Kamber, B.S., A combined Y/Ho, high field strength element (HFSE) and Nd isotope perspective on basalt weathering, Deccan Traps, India, *Chemical Geology* (2014), doi: 10.1016/j.chemgeo.2014.12.017

A combined Y/Ho, high field strength element (HFSE) and Nd isotope perspective on basalt weathering, Deccan Traps, India

Babechuk, M.G.[a,*], Widdowson, M.[b], Murphy, M.[c], and Kamber, B.S[a].

a. Department of Geology, Trinity College Dublin, Dublin 2, Ireland.

b. Department of Environment, Earth and Ecosystems, The Open University, Milton Keynes, MK7 6AA, UK

c. School of Geological Sciences, University College Dublin, Belfield, Dublin 4, Ireland

*Corresponding author contact information:

Phone: +353 (0)1 896 2675

Fax: +353 (0)1 6711199

Email: babechmg@tcd.ie

Abstract

High-precision high field strength element (HFSE: Zr, Hf, Nb, Ta, Th, U, W, Mo), Y/Ho, and Nd isotope chemostratigraphy of two contrasting Deccan Traps weathering profiles – an ancient, deeply weathered laterite, and a younger, more moderately weathered saprolite – is used to reconstruct different aspects of basalt weathering. Precision of the HFSE analyses is demonstrated through a report of the long-term concentrations and ratios determined in United States Geological Survey (USGS) and Geological Survey of Japan (GSJ) basalt rock standards (BHVO-1, BHVO-2, BIR-1, BCR-2, JB-2).

The oxyanion-forming members (U, Mo, W) are the most mobile of the considered HFSE group. Extreme loss of W, far exceeding those of U and Mo during certain stages of basalt alteration, is first reported here. The ability to strongly fractionate Mo and W during weathering may contribute to solving the unresolved mass imbalance between the crustal and marine inventories of W. By contrast, Zr, Hf, Nb, and Ta preserve the ratios of the parent basalt in the profiles due to their limited mobility; these are therefore of great potential value in reconstructing basalt flow stratigraphy and correlating lava flows in weathered flood basalt provinces. Of the HFSE, Th is not a good choice as a conservative element because it is strongly susceptible to addition of aeolian dust; this is evidenced by strong excursions in Th/Nb that are correlatable with alkali element enrichment and less radiogenic $^{143}Nd/^{144}Nd$ ratios.

The chemical fingerprints of dust were identified in a paleo-flow top of the saprolite profile, suggesting that dust accumulation occurred during periods of quiescence between basaltic eruptions. During protracted exposure and laterite development, the magnitude to which dust overprints the basalt chemistry increases substantially as evident from much less radiogenic Nd isotope ratios and higher Th/Nb ratios in the Bidar profile relative to the protolith basalt.

Attempts at quantifying the magnitude of dust accumulation in the laterite based on Th enrichment indicate a mass fraction of greater than 0.5 when the dust is assumed to have the chemistry of average upper continental crust. Although mixing models between the basalt and assumed dust composition cannot unambiguously constrain the dust source, the Nd isotope mixture preserved in the laterite points to a relatively young crustal dust source (e.g., similar to loess in composition) rather than the Precambrian shield rocks in the vicinity of the Deccan Traps. The contrasting topologies of dust-derived Nd and dust-derived Th in the laterite appears to record both physical transport of dust (Th) through permeable laterite horizons as well as transport by chemical dissolution and precipitation (Nd) at an inferred paleo-water table and in deep saprolite zones.

Yttrium and Ho fractionate substantially during all observed stages of weathering, with Y/Ho ratios ranging from 26.5 to 21.9 in the moderately weathered saprolite profile and from 30.2 to 14.7 in the laterite profile. The single strongly superchondritic Y/Ho ratio of 30.2 in the laterite is restricted to a sample at depth, and appears to fingerprint the deposition of REE derived from dissolution higher in the profile. Decrease in the Y/Ho ratio relative to the protolith basalt (24.4-24.7) in both profiles inversely correlates with chemical weathering indices, and suggests that Y/Ho ratios have significant potential as a silicate weathering proxy. Consequently, suspended vs. dissolved river loads may record the differing behaviour of these elements during weathering.

Keywords: Deccan Traps, basalt weathering, HFSE, Mo, W, dust, Nd isotopes, Y/Ho

1. Introduction

Weathering of large continental flood basalt provinces (CFBPs) represents a major sink of atmospheric carbon dioxide (Louvat and Allègre, 1997, 1998), and their long-term weathering plays an important part of the geochemical cycle of many other elements (e.g., Dessert et al., 2001, 2003). The contribution of basaltic rocks to the continental weathering flux is known to have fundamentally affected ocean chemistry because the geologically rapid (~1–4 Myr) emplacement and associated sub-aerial alteration and erosion of CFBPs such as the Deccan Traps (67–64 Ma) can be readily identified in the marine Sr and Os isotope record (e.g., Vonhof and Smit, 1997; Ravizza and Peucker-Ehrenbrink, 2003). However, such well-documented signatures serve to highlight a need to better constrain the proportion of elements delivered from these basaltic terrains, and to determine the relative contributions of the processes that release them.

Detailed geochemical investigation is crucial to understanding the modern and ancient development and evolution of the 'critical zone' – the complex, near surface environment in which rock, soil, water, air, and living organisms interact (e.g., Brantley and Lebedeva, 2011). One of the major, yet still poorly understood, processes in the geochemical evolution of the critical zone, is the accumulation and downward migration of aeolian dust. The strongest evidence for this comes from the presence of "foreign" minerals (e.g., Rex et al., 1969; Jackson et al., 1972; Kurtz et al., 2001) in the profile and isotopic compositions (e.g., Nd, Hf, Sr, or Li isotopes) that are outside the limits achievable from simple alteration of the parent rock (Borg and Banner, 1996; Kurtz et al., 2001; Kisakürek et al., 2004; Viers and Wasserburg, 2004; Pett-Ridge et al., 2009; Liu et al., 2013). Although this allochthonous input introduces an obvious complication to chemical mass balance determinations, it is becoming increasingly apparent that dust plays an important role in the long-term evolution of weathering profiles through resupplying nutrients and altering the chemical signature of

the weathering flux. Assessing the dust contribution in weathering profiles thus has the potential to help reconstruct the exposure history of landmasses and provide insight into certain paleoclimatic conditions (e.g., Brimhall et al., 1988; Chadwick et al., 1999; Vitousek, 2004).

It is generally accepted that the isotopic ratios of elements with relatively high atomic numbers, such as those of Hf and Nd (e.g. $^{143}Nd/^{144}Nd$) are not significantly fractionated by incongruent weathering (cf. Ma et al., 2010). It is for this reason that radiogenic isotope ratio variations can be used to quantify, through end-member mixing models, the mass balance between indigenous material and foreign matter such as dust in weathering profiles if they differ in chemical composition (e.g., Borg and Banner, 1996; Kurtz et al., 2001; Viers and Wasserburg, 2004). In this regard, the strongly contrasting chemistry of depleted mantle-derived basalt from that of the average upper continental crust, a typical approximation of dust, makes basalt weathering profiles an ideal substrate to fingerprint aeolian dust accumulation.

In this study, a selection of the high field strength elements (HFSE; Nb, Ta, Zr, Hf, Th, U, W, Mo, Y, Ho), those with a high charge to mass ratio, is combined with Nd isotopes to address different aspects of basalt weathering profile evolution. Analysis is performed on two profiles from the Deccan Traps, India: the deep, Paleogene Bidar laterite and a sub-Recent profile near Chhindwara that spans incipient to intermediate stages of weathering. The geology and preparatory geochemical studies of the profiles have been reported previously (Kisakürek et al., 2004; Wimpenny et al., 2008; Babechuk et al., 2014). The aim of the study is to address three central topics related to the critical zone:

1) The first pre-requisite in geochemical studies of weathering is identifying the least mobile elements during the alteration of the parent rock. The HFSE (Zr-Hf-Nb-Ta-Th) are typically

hosted in weathering-resistant minerals (e.g., Fe-Ti oxides) and exhibit generally limited solubility, apart from those that can form more soluble oxyanions (U, W, Mo). For this reason, the HFSE are often assumed to be immobile, yet this is not always the case, and they may additionally be modified by dust (e.g., Kurtz et al., 2000). In this study, ratios of the HFSE in the basalt profiles are used to assess which elements are least mobile and least influenced by dust. These elements are then used to investigate certain aspects of the pre-weathering characteristics of the basalt protolith, including fingerprinting variations in HFSE chemistry of adjacent flows and the use of HFSE in correlating flow units in lateritised regions. Next, since little is known about bedrock weathering of W and Mo, the comparative mobility of U, Mo, and W is considered. The importance of constraining their weathering behaviour is discussed in the context of their flux from the crust, both at present and in deep geological time, since both elements have importance serving a bioessential function as metal cofactors.

2) Previous studies of the Bidar laterite presented tentative geochemical evidence for dust addition to the Deccan Traps region (Mason et al., 2000; Kisakürek et al., 2004; Wimpenny et al., 2008), which is further explored in this study with more sensitive and conclusive geochemical fingerprints in the form of Nd isotopes and element Th-U-Nb-Nd systematics of the profile. An attempt is made to further resolve the magnitude of dust accumulation and the post-addition redistribution of the dust-derived components during protracted evolution of the weathering profile, which is of relevance to reconstructing the exposure and uplift history of the Deccan Volcanic Province. New evidence for dust addition during the periods of quiescence between volcanic eruptions during Deccan Traps emplacement, prior to the extended period of lateritisation, is also provided. This has significance when assessing total eruptive duration for the Deccan episode (Chenet et al., 2008).

3) The final aim of this study is to explore the weathering-related fractionation of the geochemical twin elements Y and Ho (Babechuk et al., 2012; Thompson et al., 2013). The contrasting alteration history of the geochemically similar parent basalt of the two profiles allows an evaluation of the degree of Y/Ho fractionation across a wide range of weathering conditions, and this preliminary work indicates that the this ratio has potential as a novel tracer of weathering intensity. Weathering-induced changes of Y/Ho from parent rock ratios are predicted to result in observable fractionation in derived sediments and riverine waters; this is briefly explored using a pre-existing data set of dissolved rare earth elements and yttrium (REE+Y) from rivers in eastern Australia (Lawrence et al., 2006a,b).

From a broader perspective, this study contributes to the understanding of the geochemical evolution of basaltic weathering profiles, which is relevant to reconstructing how basalt weathering has influenced ancient Earth systems. More broadly still, it may also provide a context for better understanding basalt alteration behaviour on the Martian surface (Morris et al., 2006). Further, this study also adds to mounting evidence that dust addition to weathering profiles, although most easily fingerprinted in basaltic environments, is a fundamental process in shaping the geochemistry of the critical zone and is thus of essential consideration with regards to modelling mass balance and nutrient availability.

2. Methods

2.1 High-precision trace element analysis

Trace element analysis was performed at Laurentian University, Canada, via solution quadrupole ICP-MS (SQ-ICP-MS) measurement with an XSeriesII as described below and in Babechuk et al. (2014). For sample digestion, 100 mg of sample powder was transferred into

Savillex® beakers into which a HF-HNO_3 (4:1) mixture was added. The beakers were left sealed on a hotplate at 160°C for 72 hrs and agitated at least once every 24 hrs. The residue was evaporated and the resulting fluorides were attacked with 6 N HCl (twice using 0.5 mL) and converted to nitrates using concentrated HNO_3 (twice using 1 mL) with evaporation to dryness between and following each step. The ensuing nitrate residue was dissolved in a final 10 g 20% HNO_3 stock solution. Inspection revealed no undissolved material after these steps. A calibration standard [United States Geological Survey (USGS) W-2a] and quality control standards [typically USGS and Geological Survey of Japan (GSJ) rock standards] were prepared following a similar procedure (omitting the addition of HCl after first step of digestion) and were analysed along with batches of sample unknowns. The ICP-MS analyses followed the experimental design of Eggins et al. (1997) with the modifications described in Kamber et al. (2003) and Babechuk et al. (2010), as per the following description. For analysis, an aliquot of stock solution was diluted to produce a 2% HNO_3 solution with an elemental and enriched isotope internal standard mixture containing ^{6}Li, Rh, Re, Bi, and ^{235}U in order to correct for the effects of matrix-related signal suppression and instrument drift. Immediately prior to running each batch of unknowns, two preparatory experiments were performed using the daily tuning conditions: a determination of the $^{235}U/^{238}U$ and $^{6}Li/^{7}Li$ ratios in the GSJ standard JA-3 or USGS standard AGV-2 to determine the natural contribution of the enriched isotope in the sample dilution mixture of unknowns; and, a series of pure element solutions containing Ba+Nd, Dy, and Zr to monitor the production rate of oxides with common isobaric interferences on the analytes of interest. Further details of these two steps are reported in Ulrich et al. (2010). Analyses of samples (n=15-25) were also preceded by procedural blanks, two or more separate W-2a solutions for calibration, and quality control standards. After the procedural blanks, standards and unknowns were bracketed with a drift monitor solution spaced every 5-7 samples to externally correct for

instrument drift remaining after internal standard correction. Following blank subtraction and internal standard, interference, and drift monitor correction, intensities were quantified as concentrations using the laboratory's preferred values for the USGS standard W-2a, as reported in Table 1 for the HFSE and for the other analytes as reported in Kamber et al. (2003) and Babechuk et al. (2010).

Method reproducibility and accuracy was assessed using the long-term average of USGS and GSJ standards run as unknowns (e.g., see Babechuk and Kamber, 2011 for Sm/Nd ratios). Table 1 reports the reproducibility of element (Y, Ho, Nb, Ta, Zr, Hf, Mo, W, Th, U) concentrations and ratios of relevance to the present study for mafic standards routinely analysed at Laurentian University (BHVO-1, BHVO-2, BIR-1, BCR-2, JB-2). Apart from Mo, the concentrations of the HFSE reproduce at 2% RSD (1 sigma) or better in the standards, with exception of BIR-1 which returns slightly higher RSD values due to very low concentrations. The long-term reproducibility of HFSE ratios is generally even better due to the cancelling of weigh-in and dilution errors that only affect absolute concentrations. Overall, the high level of precision indicates that: i) procedural blank levels were consistently low; ii) these elements are relatively homogeneously distributed in the powders digested at Laurentian University; and iii) that laboratory and experimental parameters such as sample dilution, instrument wash-out, and drift correction are suitable for HFSE determination even at very low concentrations (e.g., see Babechuk et al., 2010 for a discussion of factors which influence W determination). A comparison of the long-term mean concentration with literature values (Table 1) suggests that the applied W-2a concentrations used for calibration are accurate; in the event that consensus regarding the concentration of any element in W-2a evolves, all calibrated data can be recalculated relative to the presently preferred values (Table 1).

By contrast to the other HFSE, Mo exhibits a poorer precision in each of the USGS standards. Several lines of evidence point towards this being related to a more heterogeneous distribution (i.e., 'nugget effect') within individual aliquots of some standards in addition to variable levels of contamination during the production of the original USGS powders (e.g., Weis et al., 2005, 2006; Lin et al., 2000), as opposed to analytical factors such as instrument memory or a higher blank/sample ratio. Firstly, very similar HFSE concentrations (not differing by more than 2%) and ratios are measured in both BHVO-1 and BHVO-2 apart from Mo which reproduces to a much lower precision and Mo concentration differs by 127% where BHVO-2>BHVO-1 (Table 1). This was discussed in Weis et al. (2005, 2006) and was attributed to the use of hardened steel during powder production that resulted in greater contamination in the second generation standard. Comparison of our long-term mean values with those of Weis et al. (2005) suggests that the degree of Mo contamination within each standard is relatively consistent (Table 1). However, a comparison of Mo values for separate BHVO-2 aliquots reported in Kamber (2009) suggests that some, although minimal, variability remains between different BHVO-2 powder stocks. Secondly, an unexpectedly high Mo concentration is evident in BCR-2 (258,080±13950 ppb) that suggests a far more severe contamination during the production of this standard, as also noted by Weis et al. (2006). Heterogeneity of Mo in the W-2a calibration standard could also cause additional inaccuracy and imprecision. However, it is worth noting that a standard addition experiment by Baldwin et al. (2012) yielded a Mo concentration in W-2a of 424±2 ppb, identical to the laboratory's preferred calibration value (423 ppb). Furthermore, Mo data obtained with the present technique compared very favourably with Mo concentrations determined by isotope dilution of a separate aliquot (Baldwin et al., 2013).

These observations illustrate the limitations of using second generation USGS rock standards for calibration and why long-term mean values for heterogeneously distributed metals in

these standards do not accurately represent the achievable level of the method's analytical reproducibility. By contrast to these USGS standards, the GSJ standard JB-2 has a much more reproducible Mo concentration (RSD<3%) at low concentrations and suggests that these standards may not possess the same 'nugget effect', despite showing evidence for W contamination in some cases (e.g., Babechuk et al., 2010). Therefore, the reproducibility of Mo in the JB-2 standard is adopted to estimate the precision of Mo measurements in unknowns.

The HFSE data for the weathering profiles in this study are reported in Table 2 (Chhindwara) and Table 3 (Bidar), whereas the full trace element data set is reported in the Supplementary Material. Babechuk et al. (2014) previously reported and discussed a more limited suite of these trace element data (i.e., alkali, alkaline earth, rare earth elements, and Nb). It is noted that Ta, W, and Mo data are not reported for the Bidar samples since the powders were originally prepared using a tungsten carbide swing mill.

2.2 Nd isotope analysis

Chromatography and neodymium isotope analyses were conducted at the Department of Geology at University College Dublin (UCD) using a 100 mg aliquot of the sample powders and digested and converted with concentrated HNO_3 following the same procedure as described for the trace element analysis (Section 2.1; Babechuk et al., 2014). Following conversion, the residue was dissolved in 2 mL 1 N HNO_3 for use in chromatography. The chromatographic procedure followed the methods of Pin et al. (1994) and Pin and Zalduegui (1997), whereby the solution was passed over TRU Spec resin to separate the REE and then flushed directly onto LN Spec resin to purify the Nd.

Accuracy and external precision were monitored by repeated analysis of the La Jolla standard, which returned a mean $^{143}Nd/^{144}Nd$ of 0.511842 ± 8 ppm (2σ S.D., n=4) during the

experiments that is identical to the long term laboratory average with an external reproducibility of 10 ppm (2σ S.D., n=25) and consistent with previous high-precision work (e.g., Thirlwall, 1991). All Nd isotope data were normalised to a $^{146}Nd/^{144}Nd$ ratio of 0.7219. The $^{143}Nd/^{144}Nd$ ratio along with the in-run precision (2σ S.E.) are reported in Table 2 and Table 3. Neodymium and strontium isotope data were previously collected on the Bidar profile sample suite in an unpublished project (Mason, 1999; Mason et al., 2000). These new data are consistent with these previous analyses but offer improved internal precision.

2.3 Data presentation

Throughout the remaining text, all element ratios are calculated on a mass basis. Mean values are reported with one standard deviation (1σ SD) unless otherwise stated. Element mass balance calculations for each sample are calculated as the percent change (e.g., Kisakürek et al., 2004; Kurtz et al., 2000; Brimhall and Dietrich, 1987) of an element relative to the least-weathered parent rock (hereafter referred to as protolith), after normalisation to an immobile or least-mobile element from the following equation (1):

Eq.1: $\% \; change \; in \; R = \left[\frac{(R_{sample} - R_{protolith})}{R_{protolith}}\right] \times 100$

where R is the mass ratio of an element pair with the immobile element in the denominator (here taken as Nb or Ta based on the analysis in Section 4.1) and the protolith ratios are those from samples ChQB12 or BB1 for the Chhindwara and Bidar profiles, respectively. Chemical weathering indices are calculated on a molar (chemical index of alteration) or mass (index of lateritisation) basis using the major element data reported in Babechuk et al. (2014) and Kisakürek et al. (2004) that are available in the Supplementary Materials. Epsilon Nd isotope values are reported relative to the present day CHUR (chondritic uniform reservoir)

$^{143}Nd/^{144}Nd$ value of 0.512638 (Jacobsen and Wasserburg, 1980), calculated from the following equation $\varepsilon_{Nd} = [(^{143}Nd/^{144}Nd)_{sample}/(^{143}Nd/^{144}Nd)_{CHUR} - 1] \times 10000$.

3. Overview of Weathering Profiles

In situ weathering profiles should display an uninterrupted continuum of 'alteration horizons' progressing from unaltered basal bedrock, through to saprolite (e.g., Chhindwara profile) and, in the case of lateritic profiles, upward through a 'mottled zone' of oxyhydroxide accumulations, to highly indurated iron-rich duricrust capping (e.g., Bidar profile). The horizons are separated by interface zones made evident in outcrop from observable changes in colour, mineralogy and texture.

More precisely, the weathering front at the base of the profile is the junction between the unaltered bedrock (protolith) and overlying chemically weathered materials; this transition can occur over a narrow vertical interval (i.e. < 1m). Above the weathering front, a horizon containing a mixture of weathered material and unweathered 'corestones' occurs. This passes upward into a saprolitic zone in which structures and crystal pseudomorphs from the parent protolith may still be recognised. With further alteration, a microaggregated texture develops, known as the 'mottled zone', consisting of kaolinite particles along with crystals of Fe oxyhydroxides. With further maturation of the profile these develop in to nodules; this texture promotes good vertical drainage and further accelerates the alteration process. Under alternating dry and wet conditions, this zone becomes characterised by a strong accumulation of iron oxides. Upward, the nodular accumulations coalesce and interlock culminating in an indurated 'vermiform' or 'tubular' laterite comprising a massive, interlocking fretwork of Fe- (and Al-) oxides and hydroxides at the top of the profile.

3.1 Chhindwara profile

This Quaternary weathering profile spans two identifiable basalt flows in the Deccan Traps, exposed in a quarry east of Chhindwara (22° 04.213′ N, 79° 01.393′ E). Its structure and chemical composition is described in detail by Babechuk et al. (2014). The upper flow (ChQB) is fully exposed and capped with a thin (~20 cm) topsoil, whereas only the upper 215 cm of the lower flow (ChQA) is exposed. Fifteen samples were taken from the upper flow (ChQB1-ChQB12), including four samples that transect a corestone at a depth of 90 cm (ChQB9a-ChQB9d), and twelve samples from the lower flow (ChQA1-ChQA12) as summarised in Figure 2. Overall, this essentially saprolitic profile has progressed to an intermediate weathering intensity, with chemical index of alteration (CIA) values of 36-80 and oxidative mafic index of alteration values [$MIA_{(O)}$] values of 38-71 (Babechuk et al., 2014).The sample ChQB12 from a depth of 140 cm into the upper flow, and extracted using a coring drill, is adopted as the profile protolith based on position/relationship with the profile, its mineralogy (primary basaltic minerals), lowest chemical weathering index values (e.g., CIA: 36), and highest Fe(II)/Fe(III) ratio (Babechuk et al., 2014).

3.2. Bidar profile

Laterite is widespread in the Bidar region of the Deccan and, due to the resistant lateritic upper levels of the profile, forms a series of elevated mesa-like topographic features. The Bidar site is worthy of investigation since it has an important historical precedent: it was near here that Newbold (1846) first suggested that laterite developed as *in situ* (i.e. autochthonous) chemical residuum through the segregation and subsequent rearrangement of the minerals and elements originally comprising the parent rock (i.e., protolith). The investigated lateritic weathering profile is well exposed at the edge of a hillside near Bidar (17°54.87’N, 77°32.39’E), and extends down to a depth of ~ 50 metres preserving a complete progression from unaltered basalt to a highly indurated laterite at the surface; this transitions occurs

within two or three flows of the chemically uniform Ambenali Formation (Widdowson et al., 2000).

The Bidar profile is part of the high-level duricrust (Widdowson, 1997) that is interpreted to be the upper remnant of the lava pile that was subjected to a long period of intense weathering that post-dated volcanism (ca. 65 Ma), but dwindled following uplift associated with the Himalayan orogeny (ca. 50 Ma). After this point, changes in climate and hydrology resulted in the water table dropping, valley incision, and the duricrust being 'fossilised'. This presents a protracted interval of exposure (ca. 65 Ma to present) during which dust influenced the area during or after lateritisation (Mason et al., 2000; Kisakürek et al., 2004; Wimpenny et al., 2008), although the timing of dust addition and its source, as well as its fate in the profile are still poorly understood.

A total of 9 samples (BB1-BB9) were collected as part of detailed field logging of the Bidar profile; each sample was chosen to represent horizons at which there was an observable change in mineralogy or texture. This lateritic profile has progressed to an extreme end-member of weathering intensity, with chemical index of alteration (CIA) values of 37-100 and oxidative mafic index of alteration values [$MIA_{(O)}$] values of 36-99 (Babechuk et al., 2014). The sample BB1 from a depth of 50 m where the basalt shows no signs of alteration is adopted as the profile protolith; it contains similar chemical features as described above for ChQB12, including a primary basaltic mineralogy (pyroxene and plagioclase) and the lowest chemical weathering index values (e.g., CIA: ~37). Additional information on the Bidar profile samples is reported in the Supplementary Materials.

4. Results and Discussion

Results and discussion are grouped into three separate themes. Firstly, the relative mobility of the HFSE during weathering of the Deccan Traps basalt is investigated (Section 4.1), followed by the use of the least-mobile HFSE as potential chemostratigraphic 'fingerprints' for determining pre-weathering basalt stratigraphy and mass balance, and a separate discussion of comparatively more mobile HFSE (U, Mo, W). Secondly, the Th-U-Nb-REE and Nd isotope systematics are used to evaluate the dust accumulation and downward migration during weathering, and as a possible proxy for evaluating surface exposure duration; for instance, periods of repose between the arrival of successive lava flows, and longer-term exposure resulting in lateritisation (Section 4.2). Thirdly, the mobility of Y and the fractionation of Y/Ho are considered with respect to their importance in the chemical cycling of these elements within the hydrosphere and the potentiality of using Y/Ho as a proxy for oxidative weathering (Section 4.3).

4.1 High field strength elements

4.1.1 Zr, Hf, Nb, Ta, Th

The Chhindwara weathering profile is developed across two individual lava flows; the upper one (~4 m thick) is fully exposed whilst only a 2.15 m section of the lower flow is exposed. This succession was described by Babechuk et al. (2014), where it was shown that an offset in 'immobile' element concentrations (Al and Ti) and an abrupt change in the Al/Ti ratio marked the transition between the flows, highlighting a small difference in the original lava chemistries. The high-precision trace element data of this study permit a more detailed evaluation of the protolith HFSE characteristics and their behaviour during the early stages of basalt weathering.

In general, the concentration of the HFSE (Zr, Hf, Nb, Ta, Th) increases with increasing weathering intensity (i.e., greater loss of mobile major elements such as Ca, Na, and Mg)

within each of the flows. Superimposed on this, however, is an offset towards higher concentrations in the lower flow (ChQA) relative to the upper flow (ChQB), comparable to that observed for Ti (Babechuk et al., 2014). While these HFSE concentration offsets appear to also detect the variation in the two flow chemistries, we focus on ratios of these elements since they are more revealing in this regard by eliminating effects of weathering-related density or dilution/enrichment changes on the concentrations and have the additional benefit of reflecting relative mobility.

The isovalent geochemical twins (Zr-Hf and Nb-Ta) exhibit constant ratios (Zr/Hf=37.60±0.37; Nb/Ta=15.41±0.12) in all samples of the Chhindwara profile (Figure 1a,b). Relative to the inferred protolith (ChQB12), the Nb/Ta and Zr/Hf ratios do not deviate by more than 3% in all samples despite the general increase in element concentration that occurs with increasing chemical weathering intensity. This indicates that these elements exhibit near-equal extent of immobility in the profile (Kurtz et al., 2000), and, further, that these geochemical twin ratios are incapable of discriminating between the two lava flows. The latter feature is most likely because the isovalent elements are hosted in the same minerals making them less sensitive to primary magmatic differentiation processes. By contrast, when ratios of the HFSE elements with non-equal valence and different ionic radius (e.g., Hf/Ta, Zr/Nb, and Th/Nb) are inspected, a discrete ratio offset is evident between the two flows (Figure 1c) similar to Al/Ti (Babechuk et al., 2014) that also illustrates, but with greater resolution, the parental HFSE chemistry. Apart from this primary compositional offset, excursions from the constant ratio that characterises each flow are present in the three uppermost samples of the lower flow (ChQA10-ChQA12), and the uppermost sample of the top flow (ChQB11). This is most evident in the Th/Nb and Zr/Nb ratios. Our hypothesis that these samples have been modified by incorporation of dust will be discussed in Section 4.2. Excluding the potentially dust affected samples, the Hf/Ta and Th/Nb ratios display the least

intra-flow variability. The Th/Nb ratio distinguishes the lower (ChQA, n=9) from the upper (ChQB, n=14) flows with mean values of 0.209±0.003 and 0.177±0.003, respectively (corresponding to a ~20% offset in ratio). The Hf/Ta ratio ratios of 6.74±0.03 and 6.28±0.06 (corresponding to a ~7% offset in ratio) also separate the two flows. Finally, the Zr/Nb ratio is also characteristic for each flow (Figure 1c), but there is more variability within the lower flow (ChQA) compared to the upper flow (ChQB). This could indicate increased mobility of Zr (and Hf) over Nb at greater weathering intensity (Widdowson and Cox, 1996). High precision HFSE data can fingerprint individual lava flows due to the very limited mobility of these elements, but flows need to be sampled at reasonable density to achieve statistical significance.

In the more profoundly altered Bidar profile, the concentrations of Zr, Hf, and Nb are highly correlated and exhibit near-constant ratios, with the exception of the uppermost sample (BB9). For instance, Zr and Nb correlate particularly well, yielding an r^2 value of 0.999 and an average Zr/Nb of 13.05±0.32 (excluding BB9). Similarly, Zr/Hf and Hf/Nb in samples BB1 to BB8 are near-constant at 37.81±0.58 and 0.345±0.009, respectively, with a significant deviation present only in BB9 (Zr/Hf: 42.40; Hf/Nb: 0.464). The uppermost sample BB9 may have been subjected to mineral sorting, heavy mineral addition, or greater mobility of Nb over Zr and Hf in the most intensely weathered horizon of the laterite. Regardless of sample BB9, it is evident that Zr, Nb, and Hf are highly immobile, both relative to each other and during different stages of weathering, including the intense stages of lateritisation. By contrast to these elements, however, Th displays a very different behaviour that indicates selective enrichment; this is interpreted to be due to aeolian dust accumulation within the profile, as discussed in Section 4.2.

Although a clear offset in the Al/Ti ratio related to the flow transition in the Chhindwara profile was described in Babechuk et al. (2014), this ratio exhibits more intra-flow variability

by comparison with the trace HFSE (Zr-Hf-Nb-Ta-Th) ratios. The concentrations of the latter elements correlates more significantly with Ti than Al in the profile, and suggests that Al may be more susceptible to physical translocation of clay minerals or preferential leaching by comparison. In other words, it appears that Ti and the trace HFSE are less mobile and more suitable for assessing variation in the protolith chemistry.

The near equal Zr-Hf-Nb-Ta immobility in the basalt profiles in this study contrast with findings of Kurtz et al. (2000) who found more intense Zr leaching and reprecipitation at depth during the tropical weathering of Hawaiian basalt exposed to high levels of rainfall. Regardless of this difference, we agree with Kurtz et al. (2000) in promoting the use of Nb or Ta as the least-mobile elements for mass balance calculations. The limitation of mass balance calculations in profiles developed across flows of variable parental chemistry remains and is exposed with the high precision data of this study. For example, in the absence of geological evidence for a separate flow, the offset could be interpreted as preferential leaching and deposition of the HFSE in different soil horizons of a uniform protolith composition. In the case of the Chhindwara profile, the lack of a sufficiently unweathered protolith sample in the lower flow precludes a separate mass balance analysis and necessitates assumptions regarding the parental chemical composition of the mobile elements in order to calculate full profile mass gains or losses relative to the least-weathered sample (Babechuk et al., 2014).

4.1.2 Implications for flood basalt stratigraphy

The comparative Zr-Hf-Nb behaviour of the Bidar and Chhindwara profiles has important implications for the basalt lava eruption history. Although the thick (~50 metres) Bidar profile is likely to have developed across several lava flows (i.e., 2–3 units), the HFSE ratios imply that there was little inter-flow chemical variability compared to the Chhindwara profile. This indicates that minimal magmatic fractionation or crustal contamination occurred

between eruptions, consistent with the compositional uniformity exhibited by the thick (c. 500 m), uncontaminated MORB-like Ambenali Formation, which is widespread across the Main Deccan Province (MDP; Jay and Widdowson, 2008). By contrast, the Chhindwara area was peripheral to the MDP, possibly more distal from the eruptive source, and accordingly received flows only from the largest, most voluminous outpourings; this episodic arrival of lavas would allow for a greater degree of magmatic evolution and contamination between successive eruptions. This interpretation is further supported by the more juvenile $^{143}Nd/^{144}Nd$ ratios of the protolith of the Bidar profile (ε_{Nd}=4.3) compared to the apparently non-dust influenced Chhindwara flow centre (ε_{Nd}=0.2 to 0.4).

These results are consistent with those of Widdowson and Cox (1996), who demonstrated that Zr/Nb ratios could be used to map basalt stratigraphy over long distances, even when the substrate was lateritised. By extension, the ability to fingerprint variations in the stratigraphy of mafic lava flows using other HFSE is of benefit in localities where flow contacts are not necessarily identifiable, such as in ancient, metamorphosed paleosols or drill-hole samples (e.g., Millet et al., 2014). It is important to stress that in such circumstances chemical stratigraphies can only be produced from those elements from the primary magmatic inventory that are demonstrably immobile and not added to the profile from an external source during or after weathering.

4.1.3 U

By contrast with the HFSE already discussed (Zr-Hf-Nb-Ta), U commonly exhibits enhanced mobility in oxygenated environments through the formation of the uranyl ion [UO_2^{2-}] following the oxidation of U(IV) to U(VI). Within the Chhindwara profile, U mobility greater than that of the other HFSE is evident through the scatter and U loss expressed by the U/Nb ratio that is superimposed on the compositional variation between the upper and lower flow

(Figure 2b); relative to the U/Nb in the parent basalt (ChQB12: 0.0474), U loss dominates relative to Nb (lower U/Nb) within the individual flows apart from the enrichment evident within the centre of the corestone at a depth of 90 cm (ChQ9d). In addition to redistribution or loss of U originally hosted in the basalt, some U may have been introduced to the profile along with Th at the lava-flow tops and subsequently mobilised within the profile, but this is impossible to quantify at present. The U/Nb topology of the Bidar profile differs substantially from that of Chhindwara due to the far more complex and protracted evolution of the former that includes dust accumulation and fluctuating water table deposition, as discussed in Section 4.2.

4.1.4 Mo and W

Continental weathering is the most important means of delivering bioessential trace elements to the oceans. Secular changes in the flux of these elements from land have been linked with key events in early Earth history, such as the onset of sulphide weathering (e.g., Scott et al., 2008; Large et al., 2014). Continental fluxes are also affected by the dominant type of rock exposed to weathering at the Earth's surface. For example, a decrease in the Ni supply to oceans occurred after the near-complete disappearance of newly erupted very high-Mg (Ni-rich) komatiites in the Neoarchean. In addition to affecting the oceanic Ni/Fe ratio, Konhauser et al. (2009) postulated that this acted to 'starve' the methanogens, who depend on Ni for respiration, and may have helped trigger an ecological niche transition that facilitated the Great Oxidation Event (GOE). However, little is known about the behaviour of Ni during weathering throughout Earth history. Examples such as this underscore the necessity to better constrain the weathering behaviour of key bioessential elements in order to quantify their flux from the land surface.

Like U, W and Mo form soluble oxyanions, namely tungstate [WO_4^{2-}] and molybdate [MoO_4^{2-}], respectively, in natural waters. In contrast to U, however, these elements serve a biological function as metal cofactors in enzymes (e.g., Kletzin and Adams, 1996; Hille, 2002; Anbar, 2004; Andreesen and Makdessi, 2008; Wang, 2013). It is therefore possible that changes in their oceanic supplies and/or sinks may have exerted a limiting control on the evolution of oceanic biota and their respiration mechanisms. This motivated a more detailed analysis of W and Mo behaviour in the Chhindwara profile. It is worth noting, that although W behaviour in soils has been studied due to its potential for bioaccumulation and toxicity, especially in areas of anthropogenic and natural contamination (e.g., Bednar et al., 2009; Kennedy et al., 2012), little has been reported on its behaviour in saprolite (C horizon) profiles.

The W/Ta ratio vs. depth in the Chhindwara profile is illustrated in Figure 4a. The protolith W/Ta ratio (ChQB12: 0.168) is similar to that of modern MORB-type basalts (König et al., 2011; Babechuk et al., 2010). Throughout the upper flow, the W/Ta ratio ranges from 0.109 to 0.300, corresponding to up to 36% depletion and 79% enrichment relative to the protolith sample. Enrichment of W is restricted to three samples: the uppermost topsoil sample (ChQB11: 79%) and the two samples lowest in the flow (ChQB1/B2: 55-69%). In all remaining samples, which represent the main stratigraphic thickness of the flow, loss of W relative to Ta (decrease in W/Ta from the protolith) dominates. Within the lower flow, a much wider range of W/Ta ratios (0.021-0.909) is present. Although an offset in W/Ta at the flow boundary is expected, the magnitude is more difficult to assess as a result of the greater mobility exhibited by W relative to the other HFSE (Zr-Nb-Hf-Th). Nevertheless, the independent W/Ta topology of the lower flow reveals factors influencing the chemistry of W in the profile. Firstly, W enrichment is clearly evident in the samples at the paleo flow-top that also show Th enrichment. If Th enrichment derived from the addition of an

allochthonous component with trace element enriched characteristics closer to that of continental crust (Section 3.2), a parallel argument can be made for W enrichment in these horizons. Since the upper continental crust contains significantly higher W concentrations (e.g., ~1 ppm; Kamber et al., 2005) than the basalt (ChQB12: 92 ppb), the increase in W/Ta is not surprising. Secondly, a distinct trend of downwardly decreasing W/Ta ratios is evident, starting from samples ChQA8-ChQA9 (0.199-0.126; those below the dust-influenced flow-top) towards the lowest exposed samples of the flow (0.064 to 0.021 in ChQA1-ChQA3). If the original W/Ta ratio of the unweathered basalt in the lower flow was the same as in the upper flow (ChQB12: 0.168), the W/Ta ratios near the base of the flow would correspond to a W loss of ~60-90%. This suggests conditions that significantly enhanced the W mobility in the lower flow compared to the upper flow. In general, the downward decreasing concentration of Mg and abundance of zeolite minerals (due to increasing primary vesicularity towards the top of the lava flow) in the lower flow matches the topology of the W/Ta stratigraphy, suggesting these may be related to or directly influence the behaviour of W (e.g., loss of W from the breakdown of mafic minerals).

It is clear from a plot of W vs. W/Ta (Figure 4c), as well as the previously discussed Nb-Ta systematics, that the W/Ta ratio is controlled almost entirely by W mobility in the profile. The exact processes controlling the loss and retention of W, however, cannot be assessed from the elemental data alone. Nevertheless, it is likely that W was mobilised through the formation of tungstate or polytungstate species. Certain phyllosilicates, or Mn-Fe oxyhydroxides have been demonstrated to exert a primary control on the concentration of W in natural waters through pH-dependent adsorption or co-precipitation (e.g., Kunzendorf and Glasby, 1992; Johannesson et al., 2000; Gustafsson, 2003; Seiler et al., 2005; Bednar et al., 2009), which could also account for areas of W enrichment other than in the flow-tops. For example, the W-enriched samples ChQB1-ChQB2 are at the more highly weathered base of

the upper flow that shows a sharp increase in Fe^{3+}/Fe^{2+} relative to the more massive flow centre (Babechuk et al., 2014). Overall, the W geochemistry of the Chhindwara profile indicates, through the extensive loss of W in the saprolite, that W mobility may not be restricted to soil horizons and that certain stages of weathering and/or mineral phases may promote its preferential release.

The Mo/Ta ratio for the Chhindwara profile is shown in Figure 4b. The Mo/Ta ratio within the upper flow is relatively constant (0.790 ± 0.07), but similar to W, indicates loss of Mo relative to Ta with percent ratio change from the protolith of -22 to 5. Lower Mo/Ta ratios are present in the underlying flow, ranging from 0.747 to 0.500. The change in ratio within the lower flow is internally less variable and appears to indicate a lower degree of Mo mobility relative to W, suggesting that it is either hosted in more weathering-resistant minerals (e.g., Fe-Ti oxides; Arnórsson and Óskarsson, 2007) rather than sulphides/sulphide inclusions in the basalt (Voegelin et al., 2012) which are highly susceptible to oxidative weathering. Furthermore, although molybdate is highly soluble, it is similar to tungstate in that it is scavenged by Mn-Fe oxyhydroxides (Anbar and Rouxel, 2007; Arnórsson and Óskarsson, 2007; Kashiwabara et al., 2013), which could limit its flux from the profile. The Mo-W-Ta systematics of the Chhindwara profile could suggest that Mo is scavenged more readily than W in this case. The results of King et al. (2014) indicate that organic matter (OM) is also an important factor in binding Mo in soils, although complexing of Mo with OM outside of the topsoil and deeper within the saprolite is unlikely to outweigh the effects of primary mineral budget and influence of oxyhydroxides. A final factor that is also important with regards to Mo in the weathering profile is the potential for addition from allochthonous material (i.e., dust). By contrast to W, however, the samples at the flow-tops do not display Mo enrichments, suggesting that either any Mo received at the flow-tops was redistributed in preference to W or that dust-supplied Mo was not an important factor in the overall Mo

budget of the profile, but it is difficult based on the elemental data to fully address these possibilities.

It is clear that more detailed investigations of Mo geochemistry, both elemental and isotopic, of weathering profiles developed on different lithologies and across geological time are needed. The critical zone processes that control the retention or release of Mo are of particular interest to understanding the stable isotope systematics of Mo in the hydrosphere. For instance, at present, it is known that river waters are variably enriched in the heavier isotopes of Mo relative to igneous rocks and at least some of this fractionation is caused by preferential retention of lighter Mo isotopes in soils, in tandem with catchment geology variation and riverine Mo removal (Archer and Vance, 2008; Pearce et al., 2010; Neubert et al., 2011; Voegelin et al., 2012).

The results of the present study are limited in scope by only providing bulk elemental Mo and W concentrations. Taken at face value, however, it appears that a greater mobility and flux of W over Mo occurs during weathering of the Deccan Traps basalt. This finding may relate to the absence of easily weathered sulphides, but awaits a detailed micro-mineralogical investigation. It is worth noting that Arnórsson and Óskarsson (2007) showed that while Fe-Ti oxides likely host the majority of W and Mo in Icelandic basalt, the main supply of these elements to fresh waters is linked to the dissolution of plagioclase, pyroxene, and volcanic glass. Regardless, the findings of this study emphasise a major mass balance problem with respect to the Mo/W ratios in the hydrosphere. Because W and Mo have similar concentrations in the average upper continental crust (~1 ppm; e.g., Rudnick and Gao, 2003; Konig et al., 2011) and display conservative marine behaviour, it is predicted that they would have similar oceanic inventories. However, the observed concentration of Mo in seawater (~100 nmol kg^{-1}) is significantly higher than that of W (~50 pmol kg^{-1}) with an average molar Mo/W of ~2000 (Sohrin et al., 1999; Firdaus et al., 2008). The mass imbalance can be solved

if W is preferentially removed over Mo from the ocean or by invoking a greater retention of W on land. Previous studies have supported the former explanation by demonstrating the greater adsorption potential of W over Mo on some Mn-Fe oxyhydroxides and clay minerals (e.g., Sohrin et al., 1987; Kashiwabara et al., 2013; Gustafsson, 2003). However, Firdaus et al. (2008) noted that Mo/W ratios tend to increase at all stages in the crust-to-ocean pathway of the elements. Therefore, on a global scale, weathering on land must preferentially release Mo over W and that W must behave less conservatively than Mo at certain and currently unconstrained stages of aqueous transport prior to reaching the oceans. The former could, in part, be explained by the flux of both elements from land being dominated by release from substrates with a high Mo/W, such as basalt, even if the loss of W exceeds that of Mo as in the case of the Chhindwara weathering profile.

In deep geological time, the marine Mo inventory was drastically different from today's and it has been reasoned that Mo flux from land only became significant after the rise of atmospheric oxygen at the GOE, due primarily to continental sulphide weathering, such that the supply was able to exceed its withdrawal into marine sediment (Anbar et al., 2007; Scott et al., 2008; Large et al., 2014). By contrast to Mo, however, very little is known about the oceanic W supply and oceanic removal in deep time, although some modern constraints may be relevant. For instance, W flux from mid-ocean ridge hydrothermal activity seems to far exceed that of Mo (Kishida et al., 2004). If W supply, whether from hydrothermal activity or increased subaerial exposure of mafic-ultramafic rocks, had coincided with a greater W solubility, the Precambrian oceans may have had a much lower Mo/W ratio than at present. This could be supported by the observation that W-containing enzymes are a more ancient biological innovation (being present only in prokaryotes) than the comparatively more prolific Mo-containing enzymes (e.g., Andreesen and Makdessi, 2008). Thus, in order to fully address these issues, future studies of oceanic Mo inventories should also consider W, but

only after a more complete picture of the aqueous geochemical cycles of Mo and W in the modern environment has emerged.

4.2 Nd isotopes and Th as fingerprints of aeolian dust in weathering profiles

Immobile element and isotope ratios of weathering profiles have been used to calculate the mass of dust in weathering profiles under the assumption that the composition of the profile represents a mixture of the end-member composition of dust and the protolith (e.g., Chadwick et al., 1999; Kurtz et al., 2001). However, Ma et al. (2010) proposed incongruent release of radiogenic over non-radiogenic isotopes ($^{143}Nd > ^{144}Nd$ and $^{176}Hf > ^{177}Hf$) during intense basalt weathering which would invalidate the previous two-component mixing assumption. This proposal was based on deviations in the respective isotopic ratios and mass balance considerations that used Th as the immobile index element. Closer inspection of the data, however, reveals that samples nearest the soil surface exhibit excursions in Th/Nb and Th/Zr ratios that inversely correlate with the $^{176}Hf/^{177}Hf$ ratio. Thus, the proposal of preferential release of radiogenic Nd and Hf rests with the validity of Th immobility and mass conservation.

In our view, the change in Th/Nb and Th/Zr ratios is more likely caused by the addition of an extraneous component with higher Th and a lower $^{176}Hf/^{177}Hf$ ratio (both general characteristics of the average upper continental crust) and redistribution of this component within the profile. Therefore, the data presented by Ma et al. (2010) can be explained without incongruent fractionation of Hf isotopes. This likely extends to the Nd isotope values as well, although the greater mobility of Nd complicates direct correlations. This example emphasises the importance of carefully evaluating the HFSE characteristics of weathering profiles and combining trace element and isotope observations. In the present study, comparative element

immobility for Th and Nd and a lack of $^{143}Nd/^{144}Nd$ fractionation during incongruent weathering is assumed, such that correlated Th/Nb and Nd isotope excursions from basaltic protolith values are indicative of aeolian dust contamination in the basalt profiles.

4.2.1 Chhindwara profile

Apart from the HFSE ratio variation between the adjacent flows (Section 3.1.1), there are two subtle, but horizon-specific deviations in the Th/Nb ratio in the Chhindwara profile that were alluded to in previous discussion. The first is at the modern soil surface (ChQB11), where the Th/Nb ratio is higher at 0.216 when compared to the mean ratio of the remaining flow (0.178±0.003; Figure 2). The second is present in the three uppermost samples of the lower flow (ChQA10-ChQA12), where the Th/Nb ratio in ranges from 0.220-0.233 compared to the mean of 0.209±0.003 in the remaining 9 samples below. Due to the low solubility of both Th and Nb, these deviations are most plausibly explained by Th enrichment from the addition of an extraneous (allochthonous) material with a higher Th/Nb ratio. The higher Th/Nb ratios are accompanied in most samples by deviations towards lower Zr/Nb, higher W/Ta, and extreme alkali element enrichment (Babechuk et al., 2014). It was previously proposed in Babechuk et al. (2014) that the origin of the flow-top alkali element enrichment was the addition of aeolian dust. To test this hypothesis, the samples at the top of the lower flow were analysed for their Nd isotope composition. The data reveal an excursion towards slightly less radiogenic $^{143}Nd/^{144}Nd$ values, especially in sample ChQA12 nearest the paleo flow-top, relative to samples deeper in the flow (Figure 2). The isotopic deviation is subtle, but is outside of the error of the $^{143}Nd/^{144}Nd$ ratio measurement. Although alkali element enrichment can also be achieved through fluid-rock interaction, the HFSE and Nd isotope data presented here appear to eliminate this possibility, and instead provide strong support for an aeolian origin. By extension, this may argue against a metasomatic origin for alkali element enrichments in other Deccan Traps bole beds (e.g., Ghosh et al., 2006) and suggests

that high-precision Nd isotope and HFSE data may also explain the ambiguous origin of alkali element enrichment in other weathering profiles (e.g., Sheldon, 2003). Although the exact nature of the added dust is unknown, all of the chemical features are consistent with a composition similar to average upper continental crust (Table 4).

The constancy of the ratios of the least-mobile HFSE (Zr-Hf-Nb-Ta-Th) below the paleo flow-top of the lower flow (ChQA) and in the overlying upper flow (ChQB) indicates that contamination by dust at the paleo flow-top preceded the emplacement of the upper flow. Addition of dust (e.g., ash and other atmospheric particles) could have been achieved in two possible ways: it may have been introduced at the time of flow emplacement and mixed with the lava at the surface; or, it may have settled into the flow top after cooling and then percolated in the profile as far down as the base of the porous flow top breccia and associated vesiculation. Given that these flows are of the inflation pahoehoe type, rather than those characterised by surface disruption, and were emplaced remote from exposed basement lithologies, a post-eruption period of aeolian dust accumulation seems the more plausible explanation. Crucially, although the observed shift in the Nd isotope ratio is quite subtle, it nevertheless highlights the sensitivity of the basalt to overprinting and opens the possibility that such signatures may be a useful paleoclimatic fingerprint between basaltic eruptions. Further study may reveal that isotopic and trace element fingerprinting of Deccan bole beds can contribute to estimating exposure time, degree of aeolian contamination, and the history of potentially evolving dust sources.

4.2.2 Bidar profile

The depth variation of isotope ratios previously demonstrated the overprinting of the Bidar profile chemistry by dust (Mason et al., 2000; Kisakürek et al., 2004; Wimpenny et al., 2008), which is expanded on here using Th-U-Nb and Nd isotope systematics.

The Th/Nb ratio of the incipiently- to intermediately-altered saprolite (BB2-BB3: 0.0975-0.0978) is similar to that of the protolith (BB1: 0.0957), but increases significantly upwards from BB4 to BB9 reaching values as high as 0.530 (BB8). This upward change parallels the increasingly open and porous structure of the upper parts of the lateritic weathering profile. Assuming near-equivalent immobility of the two elements during chemical weathering (similar to the Chhindwara profile), increases in the Th/Nb ratio indicate selective Th enrichment. The magnitude of Th enrichment can be expressed more quantitatively using a percent change in Th/Nb ratio relative to the protolith; if Nb is assumed to have been immobile and the change in Th/Nb is attributed purely to Th addition, the most contaminated samples have experienced a 400% increase in Th relative to the protolith (Figure 3b). This is consistent with the addition of a significantly more trace element enriched source. Whereas it is likely that some Nb was also contributed from dust, the relatively low Nb content of upper continental crust and the constant Zr/Nb ratio in the Bidar laterite indicate that, in this system, it has been negligible by comparison to Th (Kurtz et al., 2001). Similar to Th/Nb, the U/Nb ratio increases progressively upwards to a value of 0.113-0.110 in BB8-BB9, with a distinct excursion in sample BB6 with U/Nb ratio of 0.776. Trends towards higher U/Nb ratios are not predicted based on the greater mobility of U relative to Nb, indicating that the U chemistry is highly influenced by dust and more complex internal cycling and deposition. In addition to the Th-U-Nb trends, significant variation with depth is expressed in the Nd isotope ratios, where the ε_{Nd} is identical in the protolith and incipient saprolite (BB1-BB2: 4.31-4.38), but decreases upwards towards significantly less radiogenic values from BB3 to BB9, following a more linear upward trend (Figure 3c). These isotope and trace element fingerprints of dust are similar to those observed in the Chhindwara flow tops and other basalt profiles (Kurtz et al., 2000, 2001), although indicate a substantially greater magnitude of contamination; this is likely a function of the protracted exposure of the laterite profile.

Quantitative assessment of the amount of dust added to a weathering profile requires reasonable knowledge of the dust composition. Outside of examples of young soil chronosequences with constrainable exposure histories (e.g., Chadwick et al., 1999; Kurtz et al., 2001), linking the fingerprint of dust in older weathering profiles to a specific source and unravelling the timing of dust addition are inherently more complicated. Nevertheless, based on the current location of the Bidar profile and the paleogeographic context of the Indian plate, two source areas of dust delivered to the Deccan Traps are deemed plausible: the exposed Archean-Proterozoic terrain outcropping to the south and east of the Deccan Volcanic Province; or, areas known to be prominent dust sources at present day (i.e., Sahara/Arabia or from the central Asia region; Grousset and Biscaye, 2005), as visualised in Figure 5.

Previous studies have determined the mass fraction of a dust-derived element in a sample (Chadwick et al., 1999; Kurtz et al., 2001) from isotope or trace element ratios, as shown for Nd and Th using equations 2 or 3, respectively, under the assumption that the ratios in both equations change from that of the basalt in the weathering profile only or primarily as a function of the added dust:

Eq. 2: $$f_{dust}^{Nd} = \left(\frac{\varepsilon_{Nd}^{sample} - \varepsilon_{Nd}^{basalt}}{\varepsilon_{Nd}^{dust} - \varepsilon_{Nd}^{basalt}}\right)$$

Eq. 3: $$f_{dust}^{Th} = \left(\frac{(\frac{Th}{X})_{sample} - (\frac{Th}{X})_{basalt}}{(\frac{Th}{X})_{dust} - (\frac{Th}{X})_{basalt}}\right)$$

where X is an immobile trace element (e.g., Nb, Ta, Zr, Hf) that is less influenced by dust input than Th.

Based on the known or assumed trace element concentration of the dust source, i.e., $[Y]_{dust}$, the concentration of the element associated with dust in the sample and the mass fraction of

dust ($fdust_Y$) can be calculated from the f_{dust}^{Y} value and the 'bulk' concentration of the element in the sample $[Y]_{sample}$ from equation 4:

Eq. 4: $fdust_Y = \left(\frac{f_{dust}^{Y} \times [Y]_{sample}}{[Y]_{dust}}\right)$

The mass of a dust-derived element (mg cm^{-2}) can be determined from the sample density (ρ) and extrapolated to horizons of defined thickness (h) in the profile using equation 5:

Eq. 5: $Y_{dust}^{mass} = f_{dust}^{Y} \times [Y]_{sample} \times \rho \times h$

The mass of each element in a horizon can then be divided by the concentration of the element in the dust source $[Y]_{dust}$ and summed for each horizon to determine the total mass of dust accreted (g dust cm^{-2}) in the profile as described in Kurtz et al. (2001).

In the Bidar profile, horizons are divided by assuming that the measurements of the first sample (BB1) represent the interval between its sample depth and that of the overlying sample (h=1200 cm) and so on to the uppermost horizon represented by BB9 and extending to the surface (h=200 cm). To apply the mixing model equations to the Bidar laterite, which is contaminated by dust from an unconstrained source, assumptions have to be made regarding the dust composition. First it is assumed that the dust had a similar *elemental* composition to the average upper continental crust as represented by a global loess compilation (Chauvel et al., 2014; Gallet et al., 1996), with a Th and Nd concentration of 10.64 and 27.21 ppm, respectively, and Th/Nb, Th/Zr, Th/Hf ratios of 0.856, 0.046, and 1.850, respectively (Table 4). These values all contrast substantially with those of the parent basalt (BB1) and are similar to the Asian dust values estimated for the allochthonous component in Hawaiian basalt (Kurtz et al., 2000, 2001; Table 4). This initial assumption is reasonable because most Th/X ratios in upper continental crust proxies agree quite well (e.g., Kamber et al., 2005) and are not dependent on the age of the crust. It is also noted that upper

crustal composites have the high Th concentration in the allochthonous end-member required to alter the Th/X ratios of the profile. Based on Th/Nb, Th/Zr, Th/Hf ratios, the calculated mass fraction of dust-derived Th increases upwards in the Bidar profile (see Figure 3e for mass fraction based on Th/Nb values) with similar overall dust accretion masses of 580, 760, and 740 g dust cm^{-2}, respectively (differences generated primarily by the variation of the Th/X ratios in BB8 and BB9). By comparison with the much thinner and younger basalt soils from Hawaii (Kurtz et al., 2001), the total amount of accreted dust added to the Bidar profile is substantially larger with a mass fraction ($fdust_{Th}$) reaching greater than 0.5 in the uppermost parts of the profile, and is due to the highly protracted development and exposure history of the laterite.

By contrast to similarity in elemental composition and Th/X ratios of potential dust sources, the Nd isotope characteristics can be more divergent. The global loess compilation has an approximate ε_{Nd} of -10 (Table 4) whereas the antiquity of the Archean-Proterozoic shield results in substantially less radiogenic Nd isotope values in trace element rich rocks (e.g., mean ε_{Nd} of -34±6 for Neoarchean granitoids and rhyolites of the Dharwar Craton; Mohan et al., 2013). With the same Nd concentration of 27.21 ppm, the effect of the less radiogenic (older) Nd dust source relative to that similar to that of the UCC would be a significantly lower dust-derived Nd input and mass fraction of dust in each sample (Figure 3e). The total mass of accreted dust calculated from a source with ε_{Nd} of -34 is 630 g dust cm^{-2}, whereas a dust source with ε_{Nd} of -10 results in a mass of 1650 g dust cm^{-2}. The dust calculations based on Nd, however, are much more highly influenced by uncertainties resulting from depletion of Nd in the basalt prior to dust accumulation, the prolonged and intense weathering history that redistributes Nd, and the unknown isotopic composition of the source. At present, we suggest that the closer agreement between the fraction of dust-derived Th (f_{dust}^{Th}) and dust-derived Nd (f_{dust}^{Nd}) from a source with ε_{Nd} of -10, especially in the uppermost horizons of the

laterite, is more consistent with the dust source being from a younger or a more diversely mixed end-member. However, it is clear that the Nd isotopes are incapable of unambiguously resolving the dust end-member at present and we propose that better constraints could be made from Hf isotope systematics due to the near-equal immobility of Hf, Zr, and Nb in the profile (Section 4.1.1).

4.2.3 The fate of dust during lateritisation

More robust estimates of dust addition (based on either Th or Nd) are principally limited by the relatively coarse sampling density throughout the Bidar profile. Rather than placing too much emphasis on the assumption that thick horizons of laterite are accurately represented by the chemistry of 9 samples, we instead focus on the qualitative chemostratigraphic trends of the dust-derived elements, which are independent of the assumed isotope composition of the dust and provide insight into the fate of dust-derived elements after addition to the profile. If the dust-derived Nd and Th had been brought in together and not separated chemically after accretion, a correlation between the f_{dust}^{Th} and f_{dust}^{Nd} in each sample would be expected (i.e., the dust-derived Th and Nd originally had the same distribution in the profile). Instead, the diverging topology with depth in the profile for f_{dust}^{Th} and f_{dust}^{Nd} (and the mass fraction of dust calculated from each; Figure 3e) as well as the percent change in Nd/Nb and Th/Nb (Figure 3d) suggests a contrasting chemical mobility of the two dust-derived elements.

The Th/Nb ratios and associated Th-based dust estimates increase only minimally in the saprolite horizons of the profile (BB2-BB4) from the protolith (BB1), but increase substantially towards the surface within the laterite horizons (BB5-BB9; Figure 3). This chemical distribution is proposed to reflect the changing morphology of the laterite profile and is consistent with dust trapping at the surface and winnowing downwards until the transition into less porous and permeable saprolite horizons. As such, a greater proportion of

the dust is retained in the upper horizons and the reduction in pore size filters the dust as it percolates down through the profile to the point that only the finest dust fraction can penetrate into the saprolite zones. In other words, the Th chemistry is interpreted to reflect primarily physical translocation of the dust in the laterite.

The Nd/Nb ratios and Nd-based dust estimates indicate a greater solubility and more complex redistribution of the REE in the laterite (Figure 3). The majority of the profile is highly depleted in Nd relative to the protolith, apart from samples BB3 (depth of 2600 cm) and BB6 (depth of 1100 cm). The isotopic composition of all samples from BB3 to BB9 indicate that they contain dust-derived Nd. Apart from the uppermost samples BB8 and BB9 it is also evident that the f_{dust}^{Nd} and mass fraction of dust calculated from Nd is higher in all samples deeper in the profile by contrast to the same parameters calculated using Th/Nb ratios (Figure 3e). These observations implicate remobilisation of the REE in the profile through dissolution and precipitation, including dust-derived Nd. The enrichment of the REE (and many other trace elements) in sample BB6 was previously inferred to represent accumulation at a paleo-water table zone (Kisakürek et al., 2004), whereas the REE enrichment in sample BB3 is interpreted to represent precipitation of secondary phosphates at a pH/porosity boundary deep in the profile (Babechuk et al., 2014; Viers and Wasserburg, 2004; Cotten et al., 1995). With regards to the deep sample (BB3), which does not contain dust-derived Th, the isotope composition independently confirms that the REE enrichment is the result of downward migration of REE, since it necessitates that at least some of the Nd was derived from the dust higher in the profile. Accordingly, it provides further evidence that the REE are hosted in a secondary phase that precipitated from weathering fluids. It also suggests that Th stayed lattice-bound to the incorporated allochthonous mineral(s) and did not penetrate as deeply into the profile. The fingerprint of dust-derived Nd at the paleo-water table is significant since it implies that the dust was present in the profile during its development and that the

table was relatively stable, such that local dissolution and precipitation of REE occurred in proximity of the horizon, which may also place important constraints on timing of dust accumulation; if the water table was only stable at the approximate position of BB6 (depth of 600 cm) prior to uplift and 'fossilisation' of the profile, an important finding of this study is that dust addition must have pre-dated, or, at the very least, overlapped in time. Thus, instead of post-'fossilisation' dust accumulation, it appears that dust must have been added during the northward journey of the Indian plate, and prior to any substantive uplift and attendant dissection of the laterite.

If U was brought in with Th, the Th/U and U/Nb ratios also appear to indicate that U was preferentially mobilised relative to Th and deposited elsewhere in the profile. The Th/U ratio of the two uppermost samples (4.15 and 4.71) is close to that of the average upper continental crust (Table 4), but the ratios are lower at greater depth in the profile. Similarly, higher U/Nb ratios than the parent basalt throughout the profile (Figure 3d) indicate that added U has altered the profile chemistry to a depth as low as 2600 cm (Sample BB3).

4.3 Y/Ho and mobility of yttrium

The weathering-induced mobility of the REE+Y is well documented (e.g., Cotten et al., 1995; Hill et al., 2000a,b; Patino et al., 2003), although it has only recently been shown that Y loss outweighs that of its geochemical twin Ho during chemical weathering, resulting in measurable Y/Ho fractionation (Babechuk et al., 2012; Thompson et al., 2013). The high-precision Y/Ho data in this study extend our understanding of their fractionation behaviour across a wide range of observed weathering intensity and we propose that Y/Ho fractionation may have potential as a chemical weathering proxy.

4.3.1 Y/Ho fractionation during basalt weathering

Protolith Y/Ho ratios of both the Bidar (BB1: 24.42) and the Chhindwara (ChQB12: 24.71) weathering profiles are lower than the average upper continental crust (e.g., 26.24±0.36; Kamber et al., 2005) and carbonaceous chondrites (25.94±0.08; Pack et al., 2007), but within the range of the values of the USGS and GSJ basalt standards (24.37-25.36; Table 1). Relative to the protolith values, however, a wide range of Y/Ho ratios occur throughout the weathering profiles (Chhindwara: 21.89 to 26.52; Bidar: 14.71 to 30.15) that indicate a significant weathering-related fractionation. The magnitude of Y/Ho fractionation appears to be linked to the degree of chemical weathering experienced by the basalt and also identifies secondary rare earth element enrichment.

During the earliest stages of basalt weathering, as represented by the Chhindwara profile, Y/Ho decreases gradually to as low as 21.89 in correlation with the loss of Ca and Na inferred from the CIA (Figure 6a). In some cases, however, the Y/Ho increases relative to the protolith basalt, most notably in the centre of the corestone (ChQB9), which could indicate preferential inward migration of Y (also seen by U; Section 4.1.3), since the ratio changes from 23.65 (ChQB9a) in the outermost section progressively to 26.52 in the corestone centre (ChQB9d). Previous work demonstrated the mobility of Y at early stages of basalt weathering (Hill et al., 2000a), which is confirmed by these results, although it is now clearer that this Y loss is measurable relative to Ho, even at a small scale.

The most highly fractionated Y/Ho ratios are found within the Bidar profile. Apart from sample BB3 (Y/Ho: 30.15), the values decrease upwards in the profile towards very low Y/Ho ratios (14.71 to 19.42). As with the less altered Chhindwara example, the overall trend of decreasing Y/Ho ratios in the laterite profile is anti-correlated with the weathering intensity (Figure 6b) – in this case, the index of lateritisation (IOL; Babechuk et al., 2014).

Thus, beyond the point of complete Ca and Na loss from the profile, Y mobility relative to Ho continues into the more extreme stages of Si loss during lateritisation. The exception to the general trend of Y loss in BB3 occurs in the same sample that is heavily REE enriched (Kisakürek et al., 2004; Babechuk et al., 2014), evident in this study based on the very high Nd/Nb ratio (Section 4.2.3). The REE pattern and Nd isotope composition of this sample both imply that the REE enrichment is due to the precipitation of elements derived from weathered basalt elsewhere in the evolving profile (Babechuk et al., 2014). This is consistent with the highly elevated Y/Ho ratio since weathering fluids would be predicted to have higher Y/Ho ratios than the basalt to mass balance the lower Y/Ho ratios in the profile.

The additional factor that needs to be considered, especially for the Bidar laterite, is the substantial dust addition to the profile during its evolution, including the REE (Section 4.2). A reasonable assumption is that the dust had, on average, a Y/Ho ratio similar to the average continental crust (~26). The extremely low Y/Ho ratios in the profile, however, must reflect one of two conditions; either the REE concentration of the dust was not high enough to influence the REE signature of the profile or that the Y was removed preferentially to Ho from both the basalt and the added dust. The Nd isotope data imply that the former factor is not dominant and, therefore, the extremely low Y/Ho in the most dust influenced parts of the profile is even more significant.

4.3.2 Y/Ho as a silicate weathering proxy

The fractionation of Y/Ho due to preferential Y loss in both basalt profiles is well beyond the ‘charge and radius’ controlled behaviour of the isovalent element pair (i.e., CHARAC; Bau, 1996), consistent with the results of Thompson et al. (2013). Extreme Y/Ho fractionation has traditionally been associated primarily with the aqueous transport of the REE (e.g., Nozaki et al., 1997; Lawrence and Kamber, 2006) or in highly evolved magmatic systems (Bau, 1996).

Given the well-established mobility of Y during weathering (e.g., Hill et al., 2000a) and the results of this study that indicate Y/Ho fractionation extends across all stages of basalt weathering, we propose that Y/Ho has potential as a silicate weathering proxy. Although it is evident that changes in Y/Ho ratio track the progressive alteration of primary minerals to pedogenic clays and oxides, the mechanisms of fractionation need to be better constrained. The findings of Thompson et al. (2013) suggest that Fe-(oxyhydr)oxides are the most important phase involved in fractionation and that the maximum separation of Y from Ho occurs at intermediate pH ranges. Therefore, the lower affinity of Y for Fe oxyhydroxides and oxides in weathering profiles generates a similar result to the reactive particle shuttle in the marine realm. This is consistent with the extreme fractionation associated with degree of Fe enrichment in the Bidar laterite. By contrast, organic matter is thought to exert a suppressing effect on Y/Ho fractionation (Thompson et al., 2013). If Fe-(oxyhydr)oxides are crucial to Y/Ho fractionation, the degree of Y loss relative to Ho may also be a function of protolith lithology (e.g., Fe-rich vs. Fe-depleted igneous rocks) or specific soil types and thus also influenced by climate. Consequently, Y/Ho fractionation may be more extensive in basalt-dominated catchments and may have potential as a tracer of Fe-oxide formation (i.e., oxidative weathering intensity) in paleosols. These aspects of the weathering behaviour of Y/Ho will be further illuminated as high-precision measurements of additional weathering profiles of different ages and compositions are undertaken.

4.3.3. Influence of weathering induced Y/Ho fractionation on river water and sediment geochemistry

If the fractionation of Y/Ho during weathering is a ubiquitous process, then mass balance predictions can be made with regards to the Y/Ho geochemistry of river waters and clastic sediments, two end-products of weathering. The first prediction is that clastic sediments should contain some evidence of fractionation through a slightly lower Y/Ho ratio than their

source rock. Based on results of this study, the degree of fractionation preserved in the sediment could be size fraction dependent and possibly be linked to the magnitude of weathering intensity experienced at source. The latter would therefore suggest more pronounced fractionation in sediments associated with tropical weathering conditions and stable cratonic environments. The second prediction is that the Y/Ho ratios of river waters should be higher than that of the source rocks. Here, we will address the second prediction based on the high-precision REE+Y data available to date.

A growing number of studies are recognising higher Y/Ho ratios than the average upper continental crust (as represented by shale) in river waters (e.g., Lawrence et al., 2006a,b; Leybourne and Johannesson, 2008; Babechuk et al., 2012; Thompson et al., 2013). This observation qualitatively supports the prediction that that river waters inherit high Y/Ho ratios from weathering fluids. The study of Thompson et al. (2013) previously suggested this link using the compilation of Canadian river water data from Leybourne and Johannesson (2008). However, these authors did not fully consider the complexities of aquatic REE+Y chemistry that may influence Y/Ho ratios outside of a potentially inherited weathering signature. These are summarised below and an initial attempt is made to define a better informed weathering-related Y/Ho pattern in the REE+Y data set from the studies of Lawrence et al. (2006a,b) on eastern Australian rivers.

Although there appears to be no systematic aquatic chemical process capable of fractionating Y and Ho in fresh (riverine) waters (Lawrence et al., 2006a), significant fractionation occurs in the estuarine environment. When fresh river water enters a strong salinity gradient, the higher particle reactivity of the HREE (including Ho) relative to the LREE (and Y) leads to the strong Y enrichment relative to Ho observed in seawater (Y/Ho: ~40-70; e.g., Bau et al., 1995, 1997; Nozaki et al., 1997; Alibo and Nozaki, 1999; Lawrence and Kamber, 2006). This is relevant to riverine Y/Ho chemistry in three main aspects. Firstly, only fresh waters

sufficiently unaffected by the estuarine salt wedge or saline groundwaters are suitable for assessing Y/Ho inherited from the local catchment. Secondly, if the local catchment geology is rich in marine authigenic sedimentary rocks (e.g. carbonates, phosphates), river waters will be biased towards higher Y/Ho. Finally, anthropogenic contamination from the local use of marine phosphate fertilisers can modify riverine Y/Ho ratios (e.g., Marx et al., 2010; Lawrence et al., 2006b).

An initial analysis of dissolved riverine REE+Y data from eastern Australia by Lawrence et al. (2006a,b) noted Y/Ho values higher than the average upper continental crust in samples remote from salinity gradients associated with estuarine or groundwater influx. The authors considered variations in local catchment geology, soil-related processes, and local use of fertilisers as possible explanations, but reasoned that the latter was most compatible with the data. To further account for these factors, the dissolved river water data of Lawrence et al. (2006a,b) were screened in this study based on conductivity/salinity and, when available, P concentration (Figure 6). The remaining samples (n=51) are believed to be least anthropogenically disturbed and least influenced by salinity-induced Y/Ho fractionation. The mean Y/Ho of this subset of samples is still superchondritic at 27.75±2.08 (Figure 6c). This appears to strengthen the case for Y/Ho fractionation occurring in soils and that the signature generated in weathering fluids may be inherited by the rivers. However, due to the complexities in fully addressing the factors influencing Y/Ho in larger rivers draining a variable catchment geology, detailed Y/Ho studies at all levels (protolith, saprolite, soil, ground and river water) of purely igneous catchments will be necessary to unambiguously fingerprint the sources of fractionation.

5. Conclusions

A combined high-precision HFSE (Zr-Hf-Nb-Ta-Th-U-W-Mo), Y/Ho, and Nd isotope study was performed on two separate basalt weathering profiles in the Deccan Traps that contrast in their degrees of alteration, their age, and time scale of their development during the Cenozoic. The findings of this study are of direct relevance to the weathering of other basaltic terrains and, importantly, to fluvial and marine chemistries and broader global elemental fluxes. It is evident that Zr, Hf, Nb, and Ta exhibit very limited mobility during alteration of the basalt and are thus of use in reconstructing pre-weathering chemical variability in the weathered lava flows. By contrast, the oxyanion forming elements (U, Mo, W) are much more mobile. The mobility of W exceeds that of Mo substantially in certain areas of the basalt profile. The findings of this study, although limited to only bulk element concentration, draw attention to a clear need to better establish the mechanisms of Mo and W mobility both during the weathering of different substrate lithologies, and from the perspective of global flux to the hydrosphere. This is necessary to understand present fluxes but primarily to illuminate Precambrian oceanic inventories of these biochemically important elements. This will require additional study of other, more ancient weathering profiles, and detailed investigation at the mineralogical scale, as well as studies focused on constraining the source of changes of Mo/W in waters throughout the stages of aqueous transport.

The influence of dust has previously shown to be important in modifying the chemistry of the Deccan Traps (Mason et al., 2000; Kisakürek et al., 2004; Wimpenny et al., 2008) as well as other CFBPs (e.g., Liu et al., 2013) and this is expanded on in the present study with Th-U-Nb and Nd isotope systematics. Dust accumulation is shown to occur even on the short time scale between successive lava flows, particularly at sites far from the main eruptive centres. During prolonged exposure to dust and synchronicity with lateritisation process, certain aspects of physical transport (e.g., distribution of dust-derived Th) and chemical dissolution of dust (e.g., distribution of dust-derived Nd) can be reconstructed in in the Bidar profile,

although current data still does not permit conclusive fingerprinting of the dust source. Extreme chemical overprinting and redistribution of dust-derived Nd was previously discovered in a lateritic profile from Southern Cameroon (Viers and Wasserburg, 2004), where it is evident that local rivers also inherit some of the resulting isotopic variation from the evolving profile. These cases make it evident that following the depletion of the majority of Nd hosted in the protolith, atmospheric resupply of the REE (and other elements) may begin to dominate the internal chemistry of the profile and progressively influence the net weathering flux. This crucial role of allochthonous element addition needs to be considered in geochemical investigations of weathering profiles. For example, although not the focus of this study, the influence of dust on Th and U (Pett-Ridge et al., 2007) becomes especially relevant when modelling weathering cycles with U-series isotopes.

The mobility of Y during chemical weathering is greater than that of the HREE and can be assessed using fractionation of Y/Ho. This study shows that Y/Ho fractionation extends across all stages of basalt weathering intensity and suggests that this parameter may be a very useful proxy for silicate weathering intensity once the mechanisms of fractionation are better established. The greater release of Y over Ho during chemical weathering may influence the dissolved chemistry of river waters (higher Y/Ho than source) and the chemistry of clastic sediments (lower Y/Ho ratios than source), but requires more high-precision data for confirmation.

Acknowledgements

Trace element analysis at Laurentian University was funded by a NSERC Discovery Grant to BSK. Collection of samples in the field by MW was supported by travel grants received from The Mineralogical Society, UK, and The Geological Society of London. Financial support to

MGB was provided by an Ussher Fellowship at Trinity College Dublin. S. Daly is thanked for allowing the use of the laboratories and TIMS at the National Centre for Isotope Geochemistry (University College Dublin) to aid the Nd isotope aspect of the study. D. Klinck is acknowledged for contributions to the study as part of his BSc thesis at Laurentian University. Insightful comments from two anonymous reviewers and the editorial handling by K. Mezger greatly improved the manuscript.

References

Alibo, D.S., Nozaki, Y., 1999. Rare earth elements in seawater: particle association, shale-normalization, and Ce oxidation. Geochimica et Cosmochimica Acta 63, 363-372.

Anbar, A.D., Molybdenum stable isotopes: observations, interpretations and directions. Reviews in Mineralogy and Geochemistry 55, 429-454.

Anbar, A.D., Rouxel, O., 2007. Metal stable isotopes in paleoceanography. Annual Reviews in Earth and Planetary Sciences 35, 717-746.

Anbar, A.D., Duan, Y., Lyons, T.W., Arnold, G.L., Kendall, B., Creaser, R.A., Kaufman, A.J., Gordon, G.W., Scott, C., Garvin, J., Buick, R., 2007. A whiff of oxygen before the Great Oxidation Event? Science 317, 1903-1906.

Andreesen, J.R., Makdessi, K., 2008. Tungsten, the surprisingly positively acting heavy metal element for prokaryotes. Annals of the New York Academy of Sciences 1125, 215-229.

Arnórsson, S., Óskarsson, N., 2007. Molybdenum and tungsten in volcanic rocks and in surface and <100^{o}C ground waters in Iceland. Geochimica et Cosmochimica Acta 71, 284-304.

Archer, C., Vance, D., 2008. The isotopic signature of the global riverine molybdenum flux and anoxia in the ancient oceans. Nature Geoscience 1, 597-600.

Babechuk, M.G., Kamber, B.S., Greig, A., Canil, D., Kodolányi, J., 2010. The behaviour of tungsten during mantle melting revisited with implications for planetary differentiation time scales. Geochimica et Cosmochimica Acta 74, 1448-1470.

Babechuk, M.G., Kamber, B.S., 2011. An estimate of 1.9 Ga mantle depletion using the high-field-strength elements and Nd-Pb isotopes of ocean floor basalts, Flin Flon Belt, Canada. Precambrian Research 189, 114-139.

Babechuk, M.G., Kamber, B.S., Widdowson, M., 2012. Yttrium mobility during weathering: implications for riverine Y/Ho. Mineralogical Magazine 76, 1443.

Babechuk, M.G., Widdowson, M., Kamber, B.S., 2014. Quantifying chemical weathering intensity and trace element release from two contrasting basalt profiles, Deccan Traps, India. Chemical Geology 363, 56-75.

Baldwin, G.J., Turner, E.C., Kamber, B.S., 2012. A new depositional model for glaciogenic Neoproterozoic iron formation: insights from the chemostratigraphy and basin configuration of the Rapitan iron formation. Canadian Journal of Earth Sciences 49, 455-476.

Baldwin, G.J., Nägler, T.F., Greber, N.D., Turner, E.C., Kamber, B.S., 2013. Mo isotopic composition of the mid-Neoproterozoic ocean: an iron formation perspective. Precambrian Research 230, 168-178.

Bau, M., 1996. Controls on the fractionation of isovalent trace elements in magmatic and aqueous systems: evidence from Y/Ho, Zr/Hf and lanthanide tetrad effect. Contributions to Mineralogy and Petrology 123, 323-333.

Bau, M., Dulski, P., Möller, P., 1995. Yttrium and holmium in South-Pacific seawater – vertical-distribution and possible fractionation mechanisms. Chemie der erde-Geochemistry 55, 1-16.

Bau, M., Möller, P., Dulski, P., 1997. Yttrium and lanthanides in eastern Mediterranean seawater and their fractionation during redox-cycling. Marine Chemistry 56, 123-131.

Bednar, A.J., Boyd, R.E., Jones, W.T., McGrath, C.J., Johnson, D.R., Chappell, M.A., Ringelberg, D.B., 2009. Investigations of tungsten mobility in soil using column tests. Chemosphere 75, 1049-1056.

Borg, L.E., Banner, J.L., 1996. Neodymium and strontium isotopic constraints on soil sources in Barbados, West Indies. Geochimica et Cosmochimica Acta 60, 4193-4206.

Brantley, S.L., Lebedeva, M., 2011. Learning to read the chemistry of regolith to understand the critical zone. Annual Review of Earth and Planetary Sciences 39, 387-416.

Brimhall, G.H., Dietrich, W.E., 1987. Constitutive mass balance relations between chemical composition, volume, density, porosity, and strain in metasomatic hydrochemical systems: Results on weathering and pedogenesis. Geochimica et Cosmochimica Acta 51, 567-587.

Brimhall, G.H., Lewis, C.J., Ague, J.J., Dietrich, W.E., Hampel, J., Teague, T., Rix, P., 1988. Metal enrichment in bauxites by deposition of chemically mature aeolian dust. Nature 333, 819-824.

Chadwick, O.A., Derry, L.A., Vitousek, P.M., Huebert, B.J., Hedin, L.O., 1999. Changing sources of nutrients during four million years of ecosystem development. Nature 397, 491-497.

Chatterjee, S., Goswami, A., Scotese, C.R., 2013. The longest voyage: Tectonic, magmatic, and paleoclimatic evolution of the Indian plate during its northward flight from Gondwana to Asia. Gondwana Research 23, 238-267.

Chauvel, C., Garçon, M., Bureau, S., Besnault, A., Jahn, B., Ding, Z., 2014. Constraints from loess on the Hf-Nd isotopic composition of the upper continental crust. Earth and Planetary Science Letters 388, 48-58.

Chenet, A.-L., Fluteau, F., Courtillot, V., G érard, M., Subbarao, K.V., 2008. Determination of rapid Deccan eruptions across the Cretaceous-Tertiary boundary using paleomagnetic secular variation: Results from a 1200-m-thick section in the Mahabaleshwar escarpment. Journal of Geophysical Research: Solid Earth 113, B04101.

Cotten, J., Le Dez, A., Bau, M., Caroff, M., Maury, R.C., Dulski, P., Fourcade, S., Bohn, M., Brousse, R., 1995. Origin of anomalous rare-earth element and yttrium enrichments in subaerially exposed basalts: evidence from French Polynesia. Chemical Geology 119, 115-138.

Dessert, C., Dupré, B., François, L.M., Schott, J., Gaillardet, J., Chakrapani, G., Bajpai, S., 2001. Erosion of Deccan Traps determined by river geochemistry: impact on the global climate and the $^{87}Sr/^{86}Sr$ ratio of seawater. Earth and Planetary Science Letters 188, 459-474.

Dessert, C., Dupré, B., Gaillardet, J., François, L.M., Allègre, C.J., 2003. Basalt weathering laws and the impact of basalt weathering on the global carbon cycle. Chemical Geology 202, 257-273.

Dickson, A.J., Cohen, A.S., 2012. A molybdenum isotope record of Eocene Thermal Maximum 2: implications for global ocean redox during the early Eocene. Paleoceanography 27, PA3230.

Eggins, S.M., Woodhead, J.D., Kinsley, L.P.J., Mortimer, G.E., Sylvester, P., McCulloch, M.T., Hergt, J.M., Handler, M.R., 1997. A simple method for the precise determination of ≥ 40 trace elements in geological samples by ICPMS using enriched isotope internal standardisation. Chemical Geology 134, 311-326.

Firdaus, M.F., Norisuye, K., Nakagawa, Y., Nakatsuka, S., Sohrin, Y., 2008. Dissolved and labile particulate Zr, Hf, Nb, Ta, Mo and W in the Western North Pacific Ocean. Journal of Oceanography 64, 247-257.

Gallet, S., Jahn, B., Torii, M., 1996. Geochemical characterization of the Luochuan loess-paleosol sequence, China, and paleoclimatic implications. Chemical Geology 133, 67-88.

Ghosh, P., Sayyed, M.R.G., Islam, R., Hundekari, S.M., 2006. Inter-basaltic clay (bole bed) horizons from Deccan traps of India: implications for paleo-weathering and paleo-climate during Deccan volcanism. Palaeogeography, Palaeoclimatology, Palaeoecology 242, 90-109.

Grousset, F.E., Biscaye, P.E., 2005. Tracing dust sources and transport patterns using Sr, Nd and Pb isotopes. Chemical Geology 222, 149-167.

Gustafsson, J.P., 2003. Modelling molybdate and tungstate adsorption to ferrihydrite. Chemical Geology 200, 105-115.

Hill, I.G., Worden, R.H., Meighan, I.G., 2000a. Yttrium: The immobility-mobility transition during basaltic weathering. Geology 28, 923-926.

Hill, I.G., Worden, R.H., Meighan, I.G., 2000b. Geochemical evolution of a paleolaterite: the Interbasaltic Formation, Northern Ireland. Chemical Geology 166, 65-84.

Hille, R., 2002. Molybdenum and tungsten in biology. Trends in Biochemical Sciences 27, 360-367.

Imai, N., Terashima, S., Itoh, S., Ando, A., 1995. 1994 Compilation of analytical data for minor and trace elements in seventeen GSJ geochemical reference samples, “igneous rock series”. Geostandards and Geoanalytical Research 19, 135-213.

Jochum, K, P., Nohl, U., Herwig, K., Lammel, E., Stoll, B., Hofmann, A., 2005. GeoReM: A new geochemical database for reference materials and isotopic standards. Geostandards and Geoanalytical Research 29, 333-338.

Jacobsen, S.B., Wasserburg, G.J., 1980. Sm-Nd isotopic evolution of chondrites. Earth and Planetary Science Letters 50, 139-155.

Jackson, M.L., Gibbons, F.R., Syers, J.K., Mokma, D.L., 1972. Eolian influence on soils developed in a chronosequence of basalts of Victoria, Australia. Geoderma 8, 147-163.

Jay, A.E., Widdowson, M., 2008. Stratigraphy, structure and volcanology of the SE Deccan continental flood basalt province: implications for eruptive extent and volumes. Journal of the Geological Society of London 165: 177-188.

Johannesson, K.H., Lyons, W.B., Graham, E.Y., Welch, K.A., 2000. Oxyanion concentrations in Eastern Sierra Nevada rivers – 3. Boron, Molybdenum, Vanadium, and Tungsten. Aquatic Geochemistry 6, 19-46.

Johannesson, K.H., Tang, J., 2009. Conservative behaviour of arsenic and other oxyanion-forming trace elements in an oxic groundwater flow system. Journal of Hydrology 378, 13-28.

Kamber, B.S., 2009. Geochemical fingerprinting: 40 years of analytical development and real world applications. Applied Geochemistry 24, 1074-1086.

Kamber, B.S., Greig, A., Schoenberg, R., Collerson, K.D., 2003. A refined solution to Earth's hidden niobium: implications for evolution of continental crust and mode of core formation. Precambrian Research 126, 289-308.

Kamber, B.S., Greig, A., Collerson, K.D., 2005. A new estimate for the composition of weathered young upper continental crust from alluvial sediments, Queensland, Australia. Geochimica et Cosmochimica Acta 69, 1041-1058.

Kashiwabara, T., Takahashi, Y., Marcus, M.A., Uruga, T., Tanida, H., Terada, Y., Usui, A., 2013. Tungsten species in natural ferromanganese oxides related to its different behaviour from molybdenum in oxic ocean. Geochimica et Cosmochimica Acta 106, 364-378.

Kennedy, A.J., Johnson, D.R., Seiter, J.M., Lindsay, J.H., Boyd, R.E., Bednar, A.J., Allison, P.G., 2012. Tungsten toxicity, bioaccumulation, and compartmentalization into organisms representing two trophic levels. Environmental Science & Technology 46, 9646-9652.

King, E.K., Thompson, A., Hodges, C., Pett-Ridge, J.C., 2014. Towards understanding temporal and spatial patterns of molybdenum in the critical zone. Procedia Earth and Planetary Science 10, 56-62.

Kisakürek, B., Widdowson, M., James, R.H., 2004. Behaviour of Li isotopes during continental weathering: the Bidar laterite profile, India. Chemical Geology 212, 27-44.

Kishida, K., Sohrin, Y., Okamura, K., Ishibashi, J. 2004. Tungsten enriched in submarine hydrothermal fluids. Earth and Planetary Science Letters 222, 819-827.

Kletzin, A., Adams, M.W.W., 1996. Tungsten in biological systems. FEMS Microbiology Reviews 18, 5-63.

König, S., Münker, C., Hohl, S., Paulick, H., Barth, A.R., Lagos, M., Pfänder, J., Büchl, A., 2011. The Earth's tungsten budget during mantle melting and crust formation. Geochimica et Cosmochimica Acta 75, 2119-2136.

Konhauser, K.O., Pecoits, E., Lalonde, S.V., Papineau, D., Nisbet, E.G., Barley, M.E., Arndt, N.T., Zahnle, K., Kamber, B.S., 2009. Oceanic nickel depletion and a methanogen famine before the Great Oxidation Event. Nature 458, 750-754.

Kunzendorf, H., Glasby, G.P., 1992. Tungsten accumulation in Pacific ferromanganese deposits. Mineralium Deposita 27, 147-152.

Kurtz, A.C., Derry, L.A., Chadwick, O.A., Alfano, M.J., 2000. Refractory element mobility in volcanic soils. Geology 28, 683-686.

Kurtz, A.C., Derry, L.A., Chadwick, O.A., 2001. Accretion of Asian dust to Hawaiian soils: Isotopic, elemental, and mineral mass balances. Geochimica et Cosmochimica Acta 65, 1971-1983.

Large, R.R., Halpin, J.A., Danyushevsky, L.V., Maslennikov, V.V., Bull, S.W., Long, J.A., Gregory, D.D., Lounejeva, E., Lyons, T.W., Sack, P.J., McGoldrick, P.J., Calver, C.R., 2014. Trace element content of sedimentary pyrite as a new proxy for deep-time ocean-atmosphere evolution. Earth and Planetary Science Letters 389, 209-220.

Lawrence, M.G., Kamber, B.S., 2006. The behaviour of the rare earth elements during estuarine mixing—revisited. Marine Chemistry 100, 147-161.

Lawrence, M.G., Greig, A., Collerson, K.D., Kamber, B.S., 2006a. Rare earth element and yttrium variability in south east Queensland waterways. Aquatic Geochemistry 12, 39-72.

Lawrence, M.G., Jupiter, S.D., Kamber, B.S., 2006b. Aquatic geochemistry of the rare earth elements and yttrium in the Pioneer River catchment, Australia. Marine and Freshwater Research 57, 725-736.

Lin, S., He, M., Hu, S., Yuan, H., Gao, S., 2000. Precise determination of trace elements in geological samples by ICP-MS using compromise conditions and fine matrix-matching strategy. Analytical Sciences 16, 1291-1296.

Liu, X.-M., Rudnick, R.L., McDonough, W.F., Cummings, M.L., 2013. Influence of chemical weathering on the composition of the continental crust: Insights from Li and Nd isotopes in bauxite profiles developed on Columbia River Basalts. Geochimica et Cosmochimica Acta 115, 73-91.

Louvat, P., Allègre, C.J., 1997. Present denudation rates on the island of Réunion determined by river geochemistry: basalt weathering and mass budget between chemical and mechanical erosions. Geochimica et Cosmochimica Acta 61, 3645-3669.

Louvat, P., Allègre, C.J., 1998. Riverine erosion rates on Sao Miguel volcanic island, Azores archipelago. Chemical Geology 148, 177-200.

Ma, J., Wei, G., Xu, Y., Long, W., 2010. Variations of Sr-Nd-Hf isotopic systematics in basalt during intensive weathering. Chemical Geology 269, 376-385.

Marx, S.K., Kamber, B.S., McGowan, H.A., Zawadzki, A., 2010. Atmospheric pollutants in alpine peat bogs record a detailed chronology of industrial and agricultural development on the Australian continent. Environmental Pollution 158, 1615-1628.

Mason, T.F.D., 1999. A combined chemical, mineralogical and isotopic study of lateritic soils from the Deccan Traps, S.W. India: implications for the processes which control laterite development. Master of Research Thesis. University of Edinburgh, U.K.

Mason, T.F.D., Widdowson, M., Ellam, R.M., Oxburgh, R., 2000. Isotopic variability of Sr and Nd in lateritic deposits from the Deccan Traps, India: evidence for an input of aeolian material to the laterites. Journal of Conference Abstracts 5, 674-675.

Millet, J., Hole, M., Jolley, D., 2014. A fresh approach to ditch cutting analysis as an aid to exploration in areas affected by large igneous province (LIP) volcanism, in: Cannon, S., Ellis, D. (Eds.) Exploration to Exploitation West of Shetlands. Geological Society, London, Special Publication 397. First published online February, 2014. http://dx.*doi.org/10.1144/SP397.2*

Mohajerin, T.J., Helz, G.R., White, C.D., Johannesson, K.H., 2014. Tungsten speciation in sulfidic waters: Determination of thiotungstate formation constants and modelling their distribution in natural waters. Geochimica et Cosmochimica Acta 144, 157-172.

Mohan, M.R., Piercey, S.J., Kamber, B.S., Sarma, D.S., 2013. Subduction related tectonic evolution of the Neoarchean eastern Dharwar Craton, southern India: New geochemical and isotopic constraints. Precambrian Research 227, 204-226.

Morris R. V., Klingelhöfer G., Schroder C., Rodionov D. S., Yen A., Ming D. W., de Souza P. A., Fleischer I., Wdowiak T., Gellert R., Bernhardt B., Evlanov E. N., Zubkov B., Foh J., Bonnes U., Kankeleit E., Gutlich P., Renz F., Squyres S. W., Arvidson R. E. 2006. Mössbauer mineralogy of rock, soil, and dust at Gusev crater, Mars: Spirit's journey through weakly altered olivine basalt on the plains and pervasively altered basalt in the Columbia Hills. *Journal of Geophysical Research* **111**:E02S13. DOI: 10.1029/2005JE002584.

Neubert, N., Heri, A.R., Voegelin, A.R., Nägler, T.F., Schlunegger, F., Villa, I.M., 2011. The molybdenum isotopic composition in river water: constraints from small catchments. Earth and Planetary Science Letters 304, 180-190.

Newbold, J.T., 1846. Summary of the geology of Southern India. VI: Laterite. Journal of the Royal Asiatic Society of Great Britain & Northern Ireland, 227-240.

Pack, A., Russell, S.S., Shelley, M.G., van Zuilen, M., 2007. Geo- and cosmochemistry of the twin elements yttrium and holmium. Geochimica et Cosmochimica Acta 71, 4592-4608.

Patino, L.C., Velbel, M.A., Price, J.R., Wade, J.A., 2003. Trace element mobility during spheroidal weathering of basalts and andesites in Hawaii and Guatemala. Chemical Geology 202, 343-364.

Pearce, C.R., Burton, K.W., Pogge von Strandmann, P.A.E., James, R.H., Gislason, S.R., 2010. Molybdenum isotope behaviour accompanying weathering and riverine transport in a basaltic terrain. Earth and Planetary Science Letters 295, 104-114.

Pett-Ridge, J.C., Monastra, V.M., Derry, L.A., Chadwick, O.A., 2007. Importance of atmospheric inputs and Fe-oxides in controlling soil uranium budgets and behaviour along a Hawaiian chronosequence. Chemical Geology 244, 691-707.

Pett-Ridge, J.C., Derry, L.A., Kurtz, A.C., 2009. Sr isotopes as a tracer of weathering processes and dust inputs in a tropical granitoid watershed, Luquillo Mountains, Puerto Rico. Geochimica et Cosmochimica Acta 73, 25-43.

Pin, C., Zalduegui, J.F.S., 1997. Sequential separation of light rare-earth elements, thorium and uranium by miniaturized extraction chromatography: application to isotopic analyses of silicate rocks. Analytica Chimica Acta 339, 79-89.

Pin, C., Briot, D., Bassin, C., Poitrasson, F., 1994. Concomitant separation of strontium and samarium-neodymium for isotopic analysis in silicate samples, based on specific extraction chromatography. Analytica Chimica Acta 298, 209-217.

Ravizza, G., Peucker-Ehrenbrink, B., 2003. The marine $^{187}Os/^{188}Os$ record of the Eocene-Oligocene transition: the interplay of weathering and glaciation. Earth and Planetary Science Letters 210, 151-165.

Rex, R.W., Syers, J.K., Jackson, M.L., Clayton, R.N., 1969. Eolian origin of quartz in soils of Hawaiian islands and in Pacific pelagic sediments. Science 163, 277-279.

Rudnick, R.L., Gao, S., 2003. Composition of the continental crust. In: Rudnick, R.L. (ed.), *The Crust (Vol. 3), Treatise on Geochemistry* (eds. Holland, H.D., Turekian, K.K.). Elsevier-Pergamon, Oxford, pp. 1-64.

Sarnthein, M., 1978. Sand deserts during glacial maximum and climatic optimum. Nature 271, 43-46.

Scott, C., Lyons, T.W., Bekker, A., Shen, Y., Poulton, S.W., Chu, W., Anbar, A.D., 2008. Tracing the stepwise oxygenation of the Proterozoic ocean. Nature 452, 456-460.

Seiler, R.L., Stollenwerk, K.G., Garbarino, J.R., 2005. Factors controlling tungsten concentrations in ground water, Carson Desert, Nevada. Applied Geochemistry 20, 423-441.

Sheldon, N.D., 2003. Pedogenesis and geochemical alteration of the Picture Gorge subgroup, Columbia River basalt, Oregon. Geological Society of America Bulletin 115, 1377-1387.

Sohrin, Y., Isshiki, K., Kuwamoto, T., Nakayama, E., 1987. Tungsten in North Pacific waters. Marine Chemistry 22, 95-103.

Sohrin, Y., Matsui, M., Nakayama, E., 1999. Contrasting behaviour of tungsten and molybdenum in the Okinawa Trough, the East China Sea and the Yellow Sea. Geochimica et Cosmochimica Acta 63, 3457-3466.

Thirlwall, M.F., 1991. Long-term reproducibility of multicollector Sr and Nd isotope ratio analysis. Chemical Geology (Isotope Geoscience Section) 94, 85-104.

Thompson, A., Amistadi, M.K., Chadwick, O.A., Chorover, J., 2013. Fractionation of yttrium and holmium during basaltic soil weathering. Geochimica et Cosmochimica Acta 119, 18-30.

Ulrich, T., Kamber, B.S., Woodhead, J.D., Spencer, L.A., 2010. Long-term observations of isotope ratio accuracy and reproducibility using quadrupole ICP-MS. Geostandards and Geoanalytical Research 34, 161-174.

Viers, J., Wasserburg, G.J., 2004. Behaviour of Sm and Nd in a lateritic soil profile. Geochimica et Cosmochimica Acta 68, 2043-2054.

Vitousek, P. M., 2004. *Nutrient cycling and limitation: Hawai'i as a model system* Princeton Environmental Issues Series 223pp.

Voegelin, A.R., Nägler, T.F., Pettke, T., Neubert, N., Steinmann, M., Pourret, O., Villa, I.M., 2012. The impact of igneous bedrock weathering on the Mo isotopic composition of stream waters: Natural samples and laboratory experiments. Geochimica et Cosmochimica Acta 86, 150-165.

Vonhof, H.B., Smit, J., 1997. High-resolution late Maastrichtian-early Danian oceanic $^{87}Sr/^{86}Sr$ record: Implications for Cretaceous-Tertiary boundary events. Geology 25, 347-350.

Wang, D., 2013. Redox chemistry of molybdenum in natural waters and its involvement in biological evolution. Frontiers in Microbiology 3, 427.

Weis, D., Kieffer, B., Maerschalk, C., Pretorius, W., Barling, J., 2005. High-precision Pb-Sr-Nd-Hf isotopic characterization of USGS BHVO-1 and BHVO-2 reference materials. Geochemistry, Geophysics, Geosystems 6, Q02002.

Weis, D., Keiffer, B., Maerschalk, C., Barling, J., de Jong, J., Williams, G.A., Hanano, D., Pretorius, W., Mattielli, N., Scoates, J.S., Goolaerts, A., Friedman, R.M., Mahoney, J.B., 2006. High-precision isotopic characterization of USGS reference materials by TIMS and MC-ICP-MS. Geochemistry, Geophysics, Geosystems 7, Q08006.

Widdowson, M., 1997. Tertiary paleosurfaces of the SW Deccan, Western India: implications for passive margin uplift. In: Widdowson, M. (Ed.), Paleosurfaces: Recognition, Reconstruction and Paleoenvironmental Interpretation, Geological Society of London Special Publications 120, pp. 221-248.

Widdowson, M., Cox, K.G., 1996. Uplift and erosion history of the Deccan Traps, India: Evidence from laterites and drainage patterns of the Western Ghats and Konkan Coast. Earth and Planetary Science Letters 137, 57-69.

Widdowson, M., Pringle, M.S., and Fernandez, O.A., 2000, A post K-T boundary (Early Palaeocene) age for Deccan-type feeder dykes, Goa, India: Journal of Petrology, 411177-1194.

Wimpenny, J., Gannoun, A., Burton, K.W., Widdowson, M., James, R.H., Gíslason, S.R., 2008. Rhenium and osmium isotope and elemental behaviour accompanying laterite formation in the Deccan region of India. Earth and Planetary Science Letters 261, 239-258.

Figure Captions

Figure 1: [Colour for web only] X-Y scatter plots of Ta-Nb (a), Hf-Zr (b), and Nb-Zr (c) for samples of the Chhindwara profile, divided into the upper flow [ChQB: dark (blue) shaded circles], lower flow [ChQA: light (green) shaded circles], and those at the current and paleo flow tops [shaded (orange) squares]. Constant Nb/Ta (15.41±0.12) and Zr/Hf (37.60±0.37) ratios across both flows indicates that the two isovalent element pairs are equally immobile and do not separately fingerprint each flow. By contrast, HFSE ratios of Zr-Hf-Nb-Ta-Th that combine elements with non-equal valence and/or more contrasting ionic radii (e.g., Zr/Nb) are unique in each flow and show excursions in the flow tops (c). However, each flow contains an internally constant HFSE ratio (e.g., Zr/Nb of 16.38±0.13 and 15.38±0.27 in the upper and lower flow, respectively) that still indicates limited mobility of this element group.

Figure 2: [Colour for web only] Chhindwara profile HFSE Th/Nb (a), U/Nb (b), Zr/Nb (c), Hf/Ta (d) and Nd isotope ($^{143}Nd/^{144}Nd$) ratios vs. depth (cm) below the modern surface. Error bars on the $^{143}Nd/^{144}Nd$ are the 2σ internal errors. The profile sketch (from Babechuk et al., 2014) illustrates the colour and texture variation between the two flows (ChQA and ChQB) and the sampling depth information. The contact between the two flows is shown on each plot as a horizontal dashed line. The HFSE ratios of the protolith basalt (ChQB12: 140 cm) are shown as a vertical lines in the plots. These selected HFSE ratios fingerprint each flow and show very limited intra-flow element mobility apart from U/Nb (due to U mobility). Deviations in most of the HFSE ratios are evident in the modern soil surface and paleo-flow surface (square symbols) denoted by the horizontal shaded horizons, which in the latter case is accompanied by a Nd isotope ratio deviation.

Figure 3: [Colour for web only] Bidar profile HFSE Zr/Nb (a), Th/Nb (b) and Nd (expressed as ε_{Nd}) isotope (c) ratios along with calculated percent change in Nd/Nb, Th/Nb, and U/Nb

ratios (d) and mass fraction of dust (e) calculated from Th and Nd chemistry. The percent change in each ratio for each sample was calculated relative to the respective ratio in the protolith (BB1), assuming that Nb was immobile during weathering, as described in the text. The mass fraction of dust ($fdust_Y$) in each sample was calculated from the elements (Y: Th or Nd) based on a dust composition (Table 4) with the following characteristics: Th/Nb ratio (0.856), Th concentration of 10.64 ppm, Nd concentration of 27.21 ppm, and an ε_{Nd} of either -10 (Chauvel et al., 2014) or -34 (Mohan et al., 2013) for the reasons described in the text (Section 4.2.2).

Figure 4: [Colour for web only] Chhindwara profile W/Ta (a) and Mo/Ta (b) ratios and a plot of W vs W/Ta ratio (c). The contact between the two flows is shown as a horizontal dashed line and the shaded areas at the tops of both flows are the areas with excursions in immobile HFSE ratios [square symbols; Figure 2]. Greater intra-flow variability in Mo/Ta and W/Ta indicates greater mobility of Mo and W relative to Ta (c) by contrast to the other HFSE (Zr-Hf-Th). This includes substantial W loss from the lower flow and areas of W enrichment relative to Ta.

Figure 5: [Colour for web only] (a) Map of modern dust sources (modified from Grousset and Biscaye, 2005, after Sarnthein, 1978) and (b) an outline of possible dust sources to the Deccan Traps during lateritisation (modified from Chatterjee et al., 2013). For the reasons discussed in the text, it is proposed that continentally-derived dust (1 or 2) with a composition similar to modern loess (e.g., Chauvel et al., 2014) is more compatible with the Bidar laterite profile chemistry than dust derived from the Archean-Proterozoic rocks exposed adjacent to the Deccan Traps (3) although the data cannot unambiguously resolve this.

Figure 6: [Colour for web only] Changes of Y/Ho in both profiles plotted against the chemical index of alteration (a) and the index of lateritisation (b), along with a comparison of

the range of Y/Ho ratios in the weathering profiles with those of dissolved river waters from the eastern Australia drainage basin (Lawrence et al., 2006a,b). The symbols in (a) and (b) are divided to show the upper flow [ChQB: dark (blue) shaded squares] and lower flow [ChQA: light (green) shaded squares] of the Chhindwara profile and the Bidar profile [dark (red) shaded circles]. For reference, the chondritic Y/Ho ratio of 25.94 from Pack et al. (2006) is shown as a broken line and the horizontal shaded area denotes the range of Y/Ho exhibit by the USGS and GSJ basalt standards and protolith basalt of this study (24.37 to 25.36). The changes of Y/Ho in the altered basalt indicate fractionation of these isovalent elements occurs during chemical weathering due to the preferential removal of Y. The data from Lawrence et al. (2006a,b) were screened to exclude samples with a salinity greater than 0.5 ‰ or conductivity greater than 150 ms/cm, and P greater than 20 ng/g to minimise the effects of salinity induced Y/Ho fractionation and phosphate fertiliser contamination. These screened data have a mean superchondritic Y/Ho ratio of 27.75±2.08 and tenuously support a mass balance with respect to the lower Y/Ho ratios generated in soils.

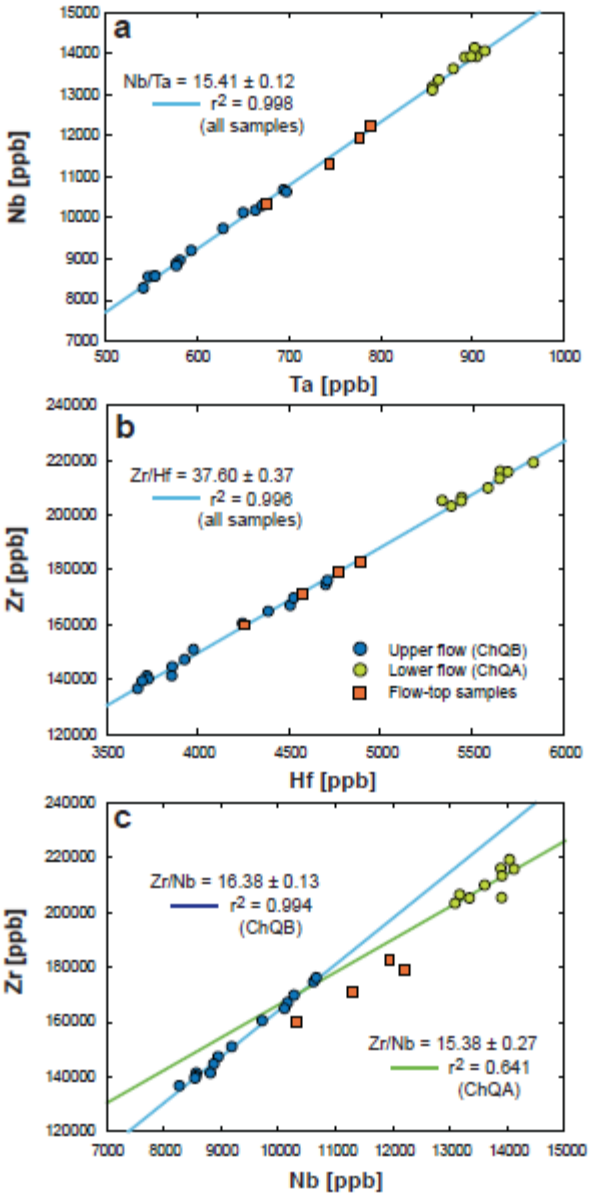

Figure 1

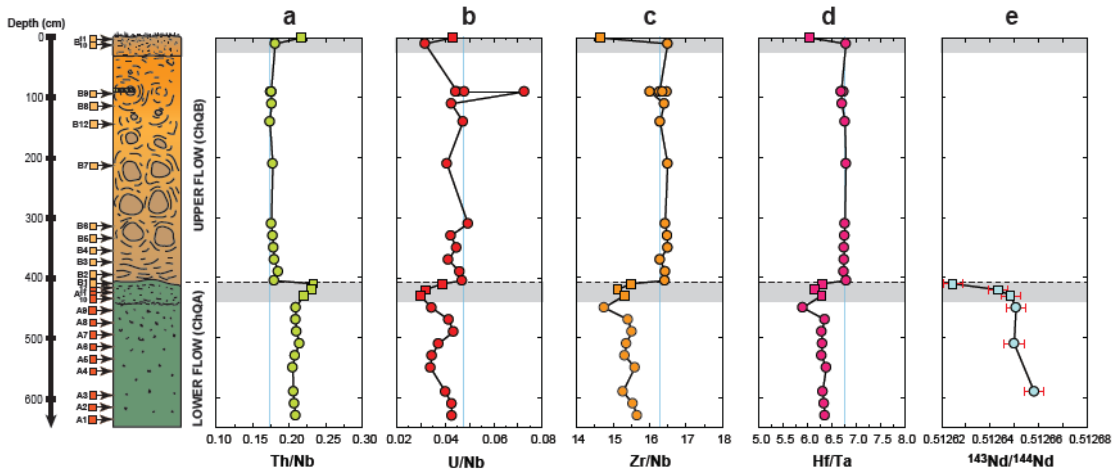

Figure 2

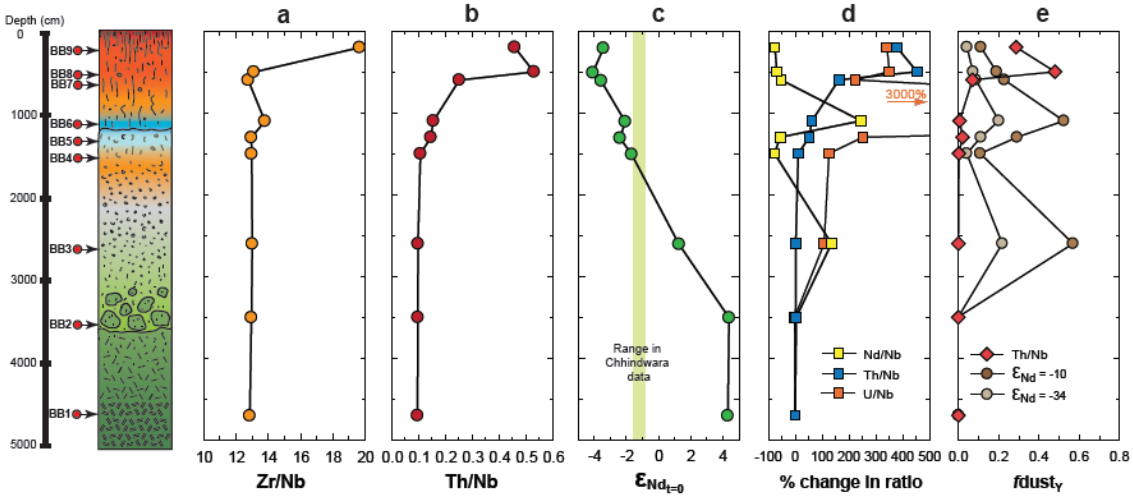

Figure 3

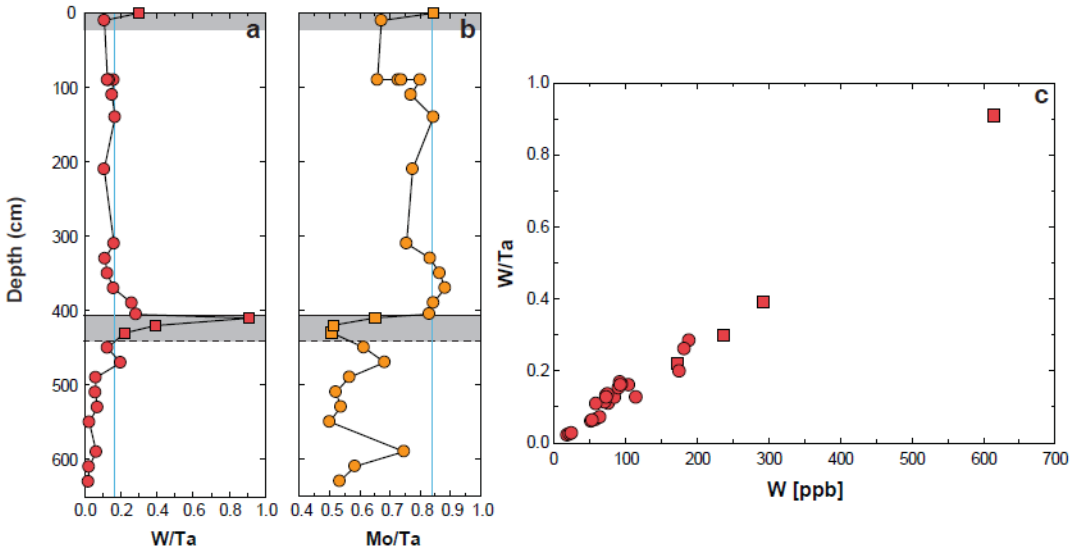

Figure 4

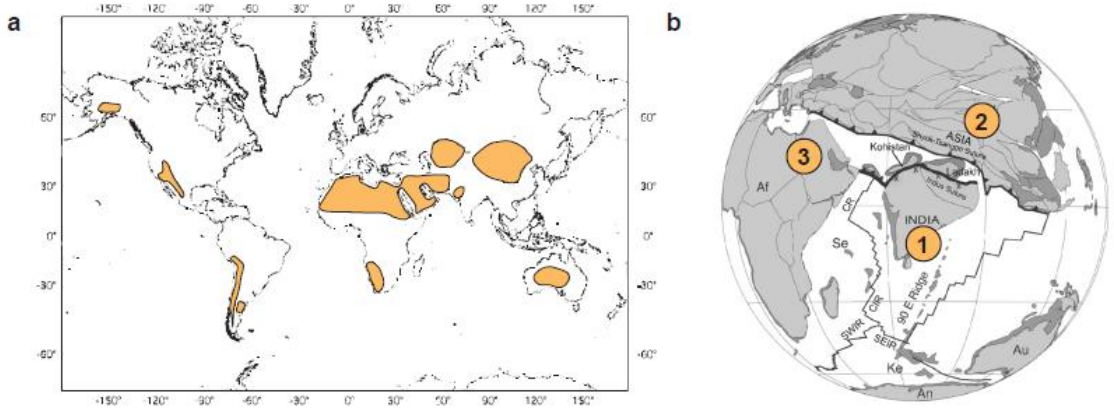

Figure 5

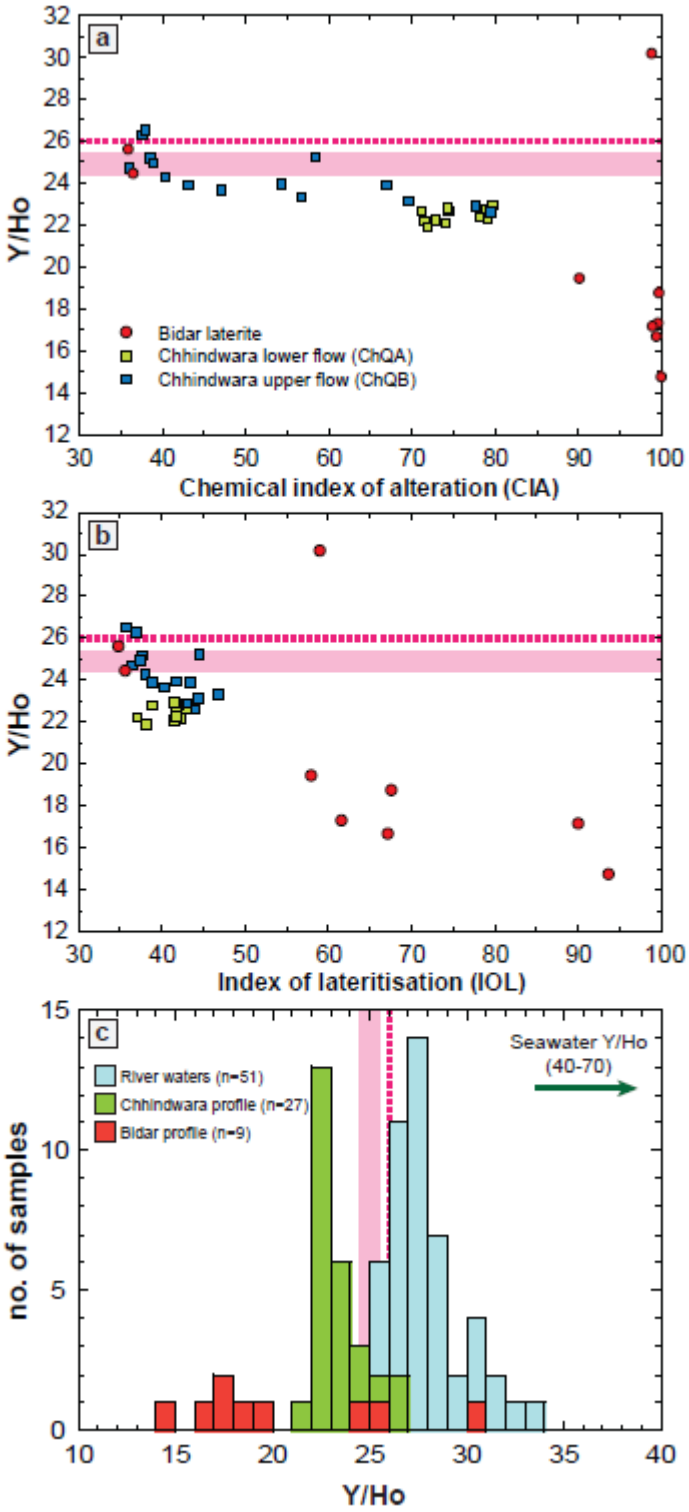

Figure 6

Table 1: Mean concentration and standard deviation (1 σ) of HFSE concentrations and ratios in basalt rock standards analysed at Laurentian University (LU)

				BHVO-1				BHVO-2				BIR-1				BCR-2				JB-2			
		W-2a	no. of digests	11				14				15				9				7			
		Calibratio	no. of analyse	43				77				38				34				20			
		n Values		LU	±	%	GeoReM	LU	±	%	GeoReM	LU	±	%	GeoReM	LU	±	%	GeoReM	LU	±	%	Literature[a]
Y	ppb	20113		24562	200	0.8	26000	24353	183	0.8	26000	14728	169	1.1	15600	33627	333	1.0	37000	22148	242	1.1	24900
Ho	ppb	803		1006	9	0.9	980	999	6	0.6	980	585	6	1.0	560	1326	12	0.9	1280	881	7	0.8	750
Nb	ppb	7275		18484	155	0.8	18600	18299	161	0.9	18100	536	8	1.4	550	12340	116	0.9	12600	489	11	2.2	1580
Ta	ppb	454		1156	9	0.8	1210	1145	10	0.9	1140	37	1	1.5	36	765	7	0.9	740	35	0	1.4	130
Zr	ppb	87866		172225	3126	1.8	174000	169345	3048	1.8	172000	14632	316	2.2	14000	185317	3025	1.6	184000	45956	1029	2.2	51200
Hf	ppb	2356		4386	81	1.8	4460	4333	66	1.5	4360	573	8	1.5	582	4846	68	1.4	4900	1450	33	2.3	1490
Th	ppb	2104		1198	17	1.4	1230	1180	13	1.1	1220	29	1	3.3	32	5783	64	1.1	5700	248	3	1.2	350
U	ppb	505		430	4	1.0	409	421	4	1.1	403	10	0	2.2	10	1699	15	0.9	1690	155	2	1.4	180
Mo	ppb	423		998	39	3.9	1000	4441	892	20	4000	40	15	39	70	258083	13948	5.4	250000	939	26	2.7	1080
W	ppb	240		193	4	2.0	210	192	4	2.2	210	6	1	9.1	7	421	6	1.3		272	7	2.7	260
Y/Ho				24.37	0.13	0.5		24.37	0.17	0.7		25.17	0.19	0.8		25.36	0.24	1.0		25.14	0.20	0.8	
Nb/Ta				15.96	0.10	0.6		15.98	0.12	0.7		14.49	0.16	1.1		16.12	0.11	0.7		14.07	0.33	2.3	
Zr/Hf				39.30	0.22	0.6		39.08	0.37	0.9		25.55	0.33	1.3		38.24	0.29	0.8		31.70	0.28	0.9	
Zr/Nb				9.318	0.17	1.9		9.262	0.15	1.6		27.282	0.59	2.2		15.018	0.23	1.5		93.917	2.48	2.6	
Hf/Ta				3.793	0.06	1.5		3.787	0.05	1.4		15.467	0.26	1.7		6.332	0.08	1.3		41.686	0.84	2.0	
Nb/Th				15.38	0.21	1.4		15.50	0.20	1.3		18.34	0.58	3.1		2.13	0.03	1.3		1.97	0.05	2.4	
Ta/W				5.976	0.10	1.6		5.959	0.11	1.9		5.078	0.56	11		1.817	0.02	1.1		0.128	0.00	2.7	
Ta/Mo				1.160	0.04	3.7		0.267	0.05	18		1.023	0.24	24		0.0030	0.0002	5.9		0.0371	0.0009	2.4	
Th/U				2.791	0.02	0.8		2.802	0.03	1.1		2.871	0.12	4.1		3.404	0.02	0.7		1.603	0.02	1.3	

Table 2: Chhindwara profile trace element ratios and Nd isotope data

Sample	Depth (cm)	$^{143}Nd/^{144}Nd$	2SE	$\varepsilon Nd_{t=0}$	Nb/Ta	Zr/Hf	Th/Nb	U/Nb	Zr/Nb	Hf/Ta	W/Ta	Mo/Ta	Y/Ho
ChQB11	0				15.48	37.57	0.2162	0.0431	14.66	6.037	0.3001	0.8443	23.35
ChQB10	10				15.37	37.38	0.1809	0.0319	16.50	6.784	0.1093	0.6719	25.22
ChQB9a	90				15.38	37.43	0.1753	0.0451	16.28	6.690	0.1604	0.8004	23.65
ChQB9b	90				15.49	37.93	0.1757	0.0480	16.47	6.727	0.1315	0.7275	24.92
ChQB9c	90				15.46	37.55	0.1744	0.0444	16.36	6.733	0.1350	0.7376	26.29
ChQB9d	90				15.28	36.59	0.1756	0.0726	16.01	6.686	0.1264	0.6590	26.52
ChQB8	110				15.49	37.92	0.1761	0.0427	16.41	6.703	0.1518	0.7699	25.17
ChQB12*	140				15.64	37.68	0.1736	0.0474	16.29	6.763	0.1681	0.8444	24.71
ChQB7	210				15.29	37.18	0.1775	0.0408	16.50	6.787	0.1083	0.7756	23.89
ChQB6	310				15.41	37.44	0.1757	0.0495	16.43	6.762	0.1623	0.7554	24.26
ChQB5	330				15.48	37.77	0.1775	0.0424	16.49	6.756	0.1126	0.8335	23.95
ChQB4	350				15.33	37.49	0.1786	0.0448	16.50	6.745	0.1259	0.8650	23.91
ChQB3	370				15.56	37.57	0.1796	0.0414	16.29	6.746	0.1602	0.8831	23.12
ChQB2	390				15.23	37.13	0.1849	0.0460	16.43	6.738	0.2607	0.8444	22.61
ChQB1	405				15.32	37.05	0.1794	0.0470	16.42	6.790	0.2840	0.8306	22.89
ChQA12	410	0.512625	0.000004	-0.26	15.30	37.64	0.2331	0.0388	15.49	6.298	0.9095	0.6513	22.81
ChQA11	420	0.512643	0.000004	0.10	15.19	37.43	0.2303	0.0319	15.13	6.139	0.3922	0.5121	22.22
ChQA10	430	0.512648	0.000004	0.20	15.37	37.44	0.2197	0.0299	15.31	6.286	0.2219	0.5064	21.89
ChQA9	450	0.512651	0.000004	0.25	15.37	38.47	0.2091	0.0345	14.75	5.895	0.1263	0.6137	22.95
ChQA8	470				15.48	37.56	0.2090	0.0415	15.41	6.350	0.1987	0.6827	22.75
ChQA7	490				15.28	37.72	0.2101	0.0435	15.51	6.285	0.0622	0.5662	22.24
ChQA6	510	0.512650	0.000004	0.23	15.45	37.69	0.2141	0.0374	15.36	6.298	0.0597	0.5208	22.38
ChQA5	530				15.47	37.74	0.2080	0.0346	15.32	6.282	0.0711	0.5375	22.86
ChQA4	550				15.36	37.56	0.2049	0.0341	15.60	6.380	0.0265	0.5002	22.07

ChQA3	590	0.512658	0.000004	0.39	15.64	37.88	0.2060	0.0402	15.27	6.307	0.0646	0.7470	22.62
ChQA2	610				15.57	38.20	0.2071	0.0428	15.54	6.333	0.0240	0.5842	22.19
ChQA1	630				15.38	37.92	0.2088	0.0428	15.66	6.350	0.0212	0.5336	22.63

* Protolith basalt

Table 3: Bidar profile trace element ratios and Nd isotope data

Sample	Depth (m)	$^{143}Nd/^{144}Nd$	2SE	$\varepsilon Nd_{t=0}$	Zr/Nb	Th/Nb	U/Nb	Nd/Nb	Y/Ho
BB9	2	0.512462	0.000003	-3.43	19.67	0.4573	0.1102	0.410	17.13
BB8	5	0.512429	0.000004	-4.08	13.11	0.5295	0.1125	0.532	18.72
BB7	6	0.512455	0.000004	-3.56	12.76	0.2515	0.0807	0.794	17.28
BB6	11	0.512532	0.000003	-2.07	13.79	0.1550	0.7760	5.779	14.71
BB5	13	0.512515	0.000004	-2.39	12.95	0.1455	0.0879	0.737	16.64
BB4	15	0.512552	0.000009	-1.67	12.97	0.1067	0.0563	0.389	19.42
BB3	26	0.512703	0.000004	1.27	13.01	0.0978	0.0517	3.934	30.15
BB2	35	0.512863	0.000003	4.38	12.96	0.0975	0.0244	1.741	25.58
BB1*	47	0.512859	0.000004	4.31	12.85	0.0957	0.0250	1.674	24.42

*Protolith basalt

Table 4: Summary of elemental (ppm) and Nd isotope compositions of the Deccan Traps basalt and possible dust sources

	Protolith basalt		Potential dust compositions				
	ChQB12	BB1	Global loess[a]	±	Asian dust[b]	AUCC[c]	±
Nd	18.27	15.51	27.21	*4.35*	26	32.91	*8.42*
Zr	139.3	119.0	267.2	*116.0*	155	198.5	*65.8*
Hf	3.70	3.16	6.61	*2.96*	4.4	5.32	*1.65*
Nb	8.55	9.26	12.82	*3.24*	15	15.33	*6.01*
Th	1.48	0.89	10.64	*2.07*	8	11.13	*4.53*
U	0.41	0.23	2.55	*0.49*		2.83	*1.50*
Th/Nb	0.174	0.096	0.856	*0.197*	0.52	0.753	*0.226*
Th/Zr	0.011	0.007	0.046	*0.018*	0.052	0.057	*0.022*
Th/Hf	0.401	0.281	1.849	*0.691*	1.8	2.103	*0.732*
U/Nb	0.047	0.025	0.206	*0.047*		0.195	*0.096*
U/Th	0.273	0.261	0.243	*0.033*		0.254	*0.066*
ε_{Nd} (t=0)		4.31	-10.3	*1.2*	-10	-3.79	*3.75*

a: Mean from loess compilation of Chauvel et al. (2014), including data from Gallet et al. (1996)
b: Asian dust composition as reported in Kurtz et al. (2000, 2001)
c: Average upper continental crust (AUCC) for comparison taken from 'MuQ' alluvial sediment compilation of Kamber et al. (2005)

Highlights

- Zr-Hf-Nb-Ta immobile and fingerprint lava flows in weathered terrains
- Extreme W mobility from basalt
- Nd isotopes and Th are sensitive to dust accumulation
- Dust-derived Th and Nd exhibit different fate based on element solubility
- Extreme Y/Ho fractionation
- Y/Ho ratios are a potential proxy for silicate weathering